HHS Public Access

Author manuscript

Sci Transl Med. Author manuscript; available in PMC 2021 May 04.

Published in final edited form as:

Sci Transl Med. 2020 May 20; 12(544): . doi:10.1126/scitranslmed.aam8572.

Selective inhibition of glycogen synthase kinase 3α corrects pathophysiology in a mouse model of fragile X syndrome

Patrick K. McCamphill[#1], **Laura J. Stoppel**[#1], **Rebecca K. Senter**[#1,†], **Michael C. Lewis**[2,‡], **Arnold J. Heynen**[1], **David C. Stoppel**[1], **Vinay Sridhar**[3], **Katie A. Collins**[2], **Xi Shi**[2], **Jen Q. Pan**[2], **Jon Madison**[2], **Jeffrey R. Cottrell**[2], **Kimberly M. Huber**[3], **Edward M. Scolnick**[2], **Edward B. Holson**[2,§], **Florence F. Wagner**[2,‖], **Mark F. Bear**[1,‖]

[1]Picower Institute for Learning and Memory, Department of Brain and Cognitive Sciences, Massachusetts Institute of Technology, Cambridge, MA 02139, USA.

[2]Stanley Center for Psychiatric Research, Broad Institute of MIT and Harvard, Cambridge, MA 02142, USA.

[3]University of Texas Southwestern Medical Center, Department of Neuroscience, Dallas, TX 75390, USA.

[#] These authors contributed equally to this work.

Abstract

Fragile X syndrome is caused by *FMR1* gene silencing and loss of the encoded fragile X mental retardation protein (FMRP), which binds to mRNA and regulates translation. Studies in the $Fmr1^{-/y}$ mouse model of fragile X syndrome indicate that aberrant cerebral protein synthesis downstream of metabotropic glutamate receptor 5 (mGluR5) signaling contributes to disease

[‖]Corresponding author. mbear@mit.edu (M.F.B.); fwagner@broadinstitute.org (F.F.W.).
[†]Present address: Flexion Therapeutics, Burlington, MA 01803, USA.
[‡]Present address: Sage Therapeutics, Cambridge, MA 02142, USA.
[§]Present address: Amathus Therapeutics, North Cambridge, MA 02139, USA.

Author contributions: P.K.M. designed and performed hippocampal electrophysiology, AGS assay, and in vivo Western blotting experiments. L.J.S. designed and performed the protein synthesis, Western blotting, inhibitory avoidance, AGS, and hyperlocomotion assays. R.K.S. designed and performed the visual cortex electrophysiology and AGS assay. M.C.L. and A.J.H. designed and performed the AGS assay. V.S., K.A.C., and K.M.H. designed and performed the electrophysiology experiments in the somatosensory cortex. J.Q.P. and X.S. designed and performed experiments in fig. S2. P.K.M., J.M., A.J.H., and J.R.C. participated in the design and execution of studies to confirm target engagement. D.C.S. contributed to study design. E.M.S., E.B.H., A.J.H., F.F.W., and M.F.B. conceived the study and participated in the design and analysis of all experiments. P.K.M., L.J.S., R.K.S., F.F.W., and M.F.B. wrote the paper.

SUPPLEMENTARY MATERIALS

stm.sciencemag.org/cgi/content/full/12/544/eaam8572/DC1

View/request a protocol for this paper from Bio-protocol..

Competing interests: MFB discloses equity in Q-State Biosciences and compensation for consulting with Q-State, Sunovion, Addex, and Biogen on various projects. M.F.B. was a cofounder of Seaside Therapeutics that developed mGluR5 negative allosteric modulators and GABA receptor agonists to treat FXS. F.F.W. consults for Biogen. F.F.W. and E.B.H. are coinventors on patent no. WO2018187630 ["Tricyclic compounds as glycogen synthase 3 (gsk3) inhibitors and uses thereof"]. E.M.S., J.R.C., F.F.W., E.B.H., M.C.L., M.F.B., L.J.S., and A.J.H. are coinventors on patent no. US20160375006 ("Uses of paralog-selective inhibitors of gsk3 kinases"). F.F.W., J.Q.P., and M.C.L. are coinventors on patent no. WO2014059383 ("Gsk3 inhibitors and uses thereof").

Data and materials availability: All data associated with this study are present in the paper or the Supplementary Materials. The compounds BRD0705, BRD3731, and BRD0320 are available from F.F.W. under a material transfer agreement with The Broad Institute of Harvard and MIT.

pathogenesis, but clinical trials using mGluR5 inhibitors were not successful. Animal studies suggested that treatment with lithium might be an alternative approach. Targets of lithium include paralogs of glycogen synthase kinase 3 (GSK3), and nonselective small-molecule inhibitors of these enzymes improved disease phenotypes in a fragile X syndrome mouse model. However, the potential therapeutic use of GSK3 inhibitors has been hampered by toxicity arising from inhibition of both α and β paralogs. Recently, we developed GSK3 inhibitors with sufficient paralog selectivity to avoid a known toxic consequence of dual inhibition, that is, increased β-catenin stabilization. We show here that inhibition of GSK3α, but not GSK3β, corrected aberrant protein synthesis, audiogenic seizures, and sensory cortex hyperexcitability in *Fmr1*$^{-/y}$ mice. Although inhibiting either paralog prevented induction of NMDA receptor–dependent long-term depression (LTD) in the hippocampus, only inhibition of GSK3α impaired mGluR5-dependent and protein synthesis–dependent LTD. Inhibition of GSK3α additionally corrected deficits in learning and memory in *Fmr1*$^{-/y}$ mice; unlike mGluR5 inhibitors, there was no evidence of tachyphylaxis or enhanced psychotomimetic-induced hyperlocomotion. GSK3α selective inhibitors may have potential as a therapeutic approach for treating fragile X syndrome.

INTRODUCTION

Fragile X syndrome (FXS) is the most prevalent inherited monogenic cause of autism and intellectual disability, affecting 1 in 4000 males and 1 in 8000 females (1–5). In most cases, FXS arises from a 5′ trinucleotide (CGG) repeat expansion that leads to hypermethylation of the *Fmr1* promoter, transcriptional silencing of the gene, and a failure to express the fragile X mental retardation protein (FMRP). FMRP is an mRNA-binding protein that has been shown to function as a translational repressor. A consistent observation in hippocampal slices from the *Fmr1*$^{-/y}$ mouse and rat models of FXS is elevated basal protein synthesis and altered protein synthesis–dependent synaptic plasticity compared to wild-type animals (6, 7). A number of strategies have been used to restore normal protein synthesis in *Fmr1*$^{-/y}$ mice, resulting in correction or amelioration of a broad constellation of mutant phenotypes (8). These findings have led to the hypothesis that a disease-modifying therapy could be developed for FXS based on rebalancing protein synthesis and synaptic function (9).

An important regulator of protein synthesis at excitatory synapses is metabotropic glutamate receptor 5 (mGluR5), and it has been proposed that many neurological and psychiatric aspects of FXS might arise from aberrant protein synthesis downstream of this receptor (10). This theory raised the possibility of targeting the synaptic signaling that leads to altered protein synthesis in FXS while leaving other signaling pathways that are unrelated to the disease intact. However, despite extensive preclinical validation of this idea (6, 8), clinical trials using mGluR5 negative allosteric modulators (NAMs) have been unsuccessful to date (11, 12). There are many reasons clinical trials fail that are unrelated to the quality of the target, but some potential limitations of the mGluR5 NAM strategy were apparent in preclinical studies. For example, in an *Fmr1*$^{-/y}$ mouse behavioral assay, there was evidence that tolerance could develop with chronic dosing (13), and in wild-type animals, it was shown that mGluR5 NAMs augment hyperlocomotion induced by psychotomimetic compounds (14, 15). The latter observation is believed to be relevant to the finding in human volunteers that a dose-limiting side effect of mGluR5 NAM treatment is derealization and

visual hallucinations (16–18). Thus, lack of durable efficacy and a narrow therapeutic window may have limited the utility of mGluR5 NAMs in FXS clinical trials. These findings highlight the importance of identifying alternative therapeutic targets for treatment of FXS.

An alternative target of potential interest in FXS is glycogen synthase kinase 3 (GSK3). Inhibitory phosphorylation of GSK3 is reduced in *Fmr1*$^{-/y}$ mice (19), and this biochemical phenotype is corrected by treatment with an mGluR5 NAM (20). Several treatments that inhibit GSK3 have been shown to correct mutant phenotypes in FXS animal models (21). For example, inhibition of GSK3 has been proposed to account for the beneficial effects of lithium treatment in FXS mouse (22, 23) and fly (20, 24–27) models. Again, however, translating these findings to the clinic has proven challenging. Although results in an open-label trial were suggestive of benefit in FXS (28), numerous side effects limit the potential of lithium as a therapeutic in children and adolescents with FXS and other autism spectrum disorders (29). To overcome the limitations of lithium, attempts have been made to develop selective GSK3 inhibitors. Although compounds such as AR-A014418 (30) and SB216763 (31) can inhibit GSK3 and ameliorate FXS phenotypes in animal models (21), they do not have kinome selectivity (32, 33) and have toxicity that prevents chronic human use. Of particular concern, these and related GSK3 inhibitors stabilize β-catenin and activate gene expression and therefore can potentially stimulate malignant growth (34–36). However, lithium treatment in patients with bipolar disorder is not associated with increased cancer incidence (37, 38), presumably related to the modest inhibition of GSK3 (<75% inhibition of total GSK3 protein) (39). The opportunity therefore exists to develop therapeutically viable, selective GSK3 inhibitors.

GSK3 has two paralogs, GSKα and GSKβ, which are derived from different genes (40). Despite sharing 67% overall sequence homology and 95% amino acid sequence identity within their adenosine triphosphate–binding domains, these paralogs have some nonredundant actions within cells (40–42). Mice lacking both alleles of GSK3α are viable, whereas deletion of GSK3β is embryonic lethal (43–45). Of particular interest, deletion of either GSK3α or β alone had no effect on the level of β-catenin in embryonic stem cells. Increased β-catenin and gene transcription required silencing of three of four GSK3 alleles (46). These findings raise the intriguing possibility that toxicity could be avoided with paralog-selective inhibitors. Although inhibitory phosphorylation of both paralogs is reduced in *Fmr1*$^{-/y}$ mice (19), a paralog-specific contribution of GSK3 to the pathophysiology of FXS has not been examined.

Recently, taking advantage of an $Asp^{133} \rightarrow Glu^{196}$ "switch" in the hinge-binding region between GSK3α and GSK3β, we developed a set of paralog-selective GSK3α, GSK3β, and GSK3α/β inhibitors. These inhibitors are about 10-fold selective for each paralog and importantly also display exquisite kinase specificity within the greater kinome (47). The development of these selective inhibitors of GSK3α and GSK3β has given us the opportunity to unambiguously evaluate the specific contribution of each paralog to the pathophysiology of FXS in *Fmr1*$^{-/y}$ mice. Inhibition of GSK3α but not GSK3β abrogated excessive protein synthesis and mGluR5-dependent long-term depression (LTD) in hippocampal slices from *Fmr1*$^{-/y}$ mice, ameliorated susceptibility to audiogenic seizures (AGS), and corrected sensory cortex hyperexcitability. Inhibition of GSK3α also reversed

deficits in learning and memory in *Fmr1*$^{-/y}$ mice without development of tolerance or enhanced psychotomimetic-induced hyperlocomotion.

RESULTS

Development of paralog-selective inhibitors of GSK3α and GSK3β

An isochemogenic, or chemically matched, set of inhibitors selective for GSK3α {BRD0705 [(*S*)-4-ethyl-7,7-dimethyl-4-phenyl-1,2,4,6,7,8-hexahydro-5*H*-pyrazolo[3,4-*b*]quinolin-5-one]}, GSK3β {BRD3731 [(*S*)-4,7,7-trimethyl-3-neopentyl-4-phenyl-1,2,4,6,7,8-hexahydro-5*H*-pyrazolo[3,4-*b*]quinolin-5-one]}, or pan GSK3α/β {BRD0320 [(*S*)-3-cyclopropyl-4,7,7-trimethyl-4-phenyl-1,2,4,6,7,8-hexahydro-5*H*-pyrazolo[3,4-*b*]quinolin-5-one]} (fig. S1) were designed through a rational structure-based approach exploiting a previously undescribed difference in the hydrogen bond network on the backside of the kinase hinge-binding domain. Each paralog-selective inhibitor had an about 10-fold selectivity for either GSK3α (BRD0705) or GSK3β (BRD3731) in a mobility shift microfluidic assay using purified enzymes (47). After noting the selectivity in this in vitro assay, we next probed the phosphorylation status and expression of Wnt signaling protein, β-catenin (fig. S2A), and the PI3K/Akt signaling protein, collapsin response mediator protein 2 (CRMP2) (fig. S2B), to test whether the paralog selectivity would translate to a cell-based assay using SH-SY5Y cultured cells. As shown in fig. S2, treating the cells with the dual inhibitor BRD0320 (10 μM) for 24 hours led to an expected increase in β-catenin. However, when the cells were treated with each of the selective inhibitors, BRD0705 and BRD3731, at 10 μM, we observed no effect on β-catenin despite inhibition of GSK3α and GSK3β, respectively, as measured by the decrease of CRMP2 phosphorylation (p-CRMP2) (fig. S2, A and B).

These inhibitors were then tested for their pharmacokinetic properties (fig. S3). C57BL/6 mice were dosed intraperitoneally (ip) with a 30 mg/kg dose of each of the compounds. Plasma, brain, and cerebrospinal fluid (CSF) samples were collected for up to 24 hours after dosing. At this dose, each compound was present in the brain at a concentration above their in vitro half-maximal inhibitory concentration (IC_{50}) for at least 4 hours after dosing. These results suggested that we could test each compound for their effects on various behaviors or phenotypes known to occur in the *Fmr1*$^{-/y}$ mouse model of FXS.

GSK3α inhibition reduces susceptibility to AGS in *Fmr1*$^{-/y}$ mice

Susceptibility to AGS is a robust and reproducible phenotype in *Fmr1*$^{-/y}$ mice that is thought to mimic hypersensitivity to environmental stimuli seen in individuals with FXS (13, 48, 49). In this assay, mice are exposed to a loud auditory stimulus (125-dB alarm), which often results in the induction of seizure-like behavior in *Fmr1*$^{-/y}$ mice, including wild running, status epilepticus, and sometimes death (>80% incidence). Treatment with lithium (20) or nonselective inhibitors of GSK3 (19) has been shown previously to protect *Fmr1*$^{-/y}$ mice from AGS. To evaluate the contribution of GSK3α and GSK3β to the development of AGS, we acutely dosed *Fmr1*$^{-/y}$ mice and wild-type littermate controls with either vehicle [10% dimethyl sulfoxide (DMSO), 45% polyethylene glycol 400 (PEG 400), and 45% normal saline] or each inhibitor within our set, BRD0705, BRD3731, or BRD0320 (30 mg/kg ip), 1

hour before exposure to the auditory stimulus (Fig. 1A and data file S1). *Fmr1*$^{-/y}$ mice treated with vehicle were significantly more likely to exhibit seizure activity in response to the stimulus compared with wild-type controls ($P = 0.001$; Fig. 1B). In accordance with the conclusions of previous studies, dual inhibition of GSK3α/β reduced seizure incidence in *Fmr1*$^{-/y}$ mice (fig. S4). We also observed a significant reduction in seizure incidence with selective inhibition of GSK3α (BRD0705) ($P = 0.02$; Fig. 1C). However, GSK3β-selective inhibition with BRD3731 yielded no significant reduction in seizure activity (Fig. 1D). In an additional cohort of mice, we injected BRD3731 or vehicle daily for five consecutive days (fig. S5). This protocol was based on the observation that daily injections of lithium over 5 days effectively reduce AGS in *Fmr1*$^{-/y}$ mice (19). Again, however, animals treated with BRD3731 exhibited seizures in response to the auditory stimulus. These findings suggest that GSK3α may be the relevant paralog contributing to AGS susceptibility seen in *Fmr1*$^{-/y}$ mice.

BRD0705 reduces exaggerated protein synthesis in *Fmr1*$^{-/y}$ mice

One of the most reproducible phenotypes in the *Fmr1*$^{-/y}$ mouse and rat is exaggerated basal protein synthesis in the hippocampus (7, 48–52). Because FMRP normally acts as a translational repressor, this biochemical phenotype has been suggested to reflect a core cause of pathophysiology in the FXS brain. It has been shown previously that chronic treatment with dietary lithium reduces elevated rates of cerebral protein synthesis in *Fmr1*$^{-/y}$ mice (23), suggesting the possibility that inhibition of GSK3 could ameliorate this phenotype. To examine the consequence of GSK3α and GSK3β inhibition on translation, we performed metabolic labeling in wild-type and *Fmr1*$^{-/y}$ mouse hippocampal slices in the presence of 10 μM BRD0705 or BRD3731 (Fig. 2A). We found that the GSK3α inhibitor (Fig. 2B) corrected elevated protein synthesis whereas the GSK3β inhibitor did not (Fig. 2C).

BRD0705 corrects cortical hyperexcitability

Increased excitability in the cerebral cortex is another robust and reproducible FXS phenotype that can be corrected by inhibition of mGluR5 or downstream signaling pathways coupled to translation (49, 53, 54). To examine the consequence of GSK3α and GSK3β inhibition on cortical excitability, we prepared slices of the visual cortex from wild-type and *Fmr1*$^{-/y}$ animals and evoked action potentials in layer 5 pyramidal neurons using white matter stimulation as described by Osterweil *et al.* (49). Responses were collected every 30 s for 30 min in vehicle, followed by an additional 30 min in the presence of either 10 μM BRD0705 or 10 μM BRD3731 (Fig. 3A). In agreement with previous studies, the number of action potentials evoked in *Fmr1*$^{-/y}$ mouse cortical slices was greater than that in wild-type slices under vehicle conditions ($P = 0.007$). Acute application of BRD0705 significantly dampened this excessive activity in *Fmr1*$^{-/y}$ slices without affecting wild-type slices ($P = 0.0047$; Fig. 3, B to D). Application of BRD3731, however, did not alter activity in wild-type or *Fmr1*$^{-/y}$ slices (fig. S6). We also observed that *Fmr1*$^{-/y}$ mouse visual cortical slices displayed enhanced spontaneous firing and that BRD0705, but not BRD3731, significantly dampened this aberrant activity ($P = 0.0001$; Fig. 4, A to C, and fig. S7).

In the somatosensory cortex of *Fmr1*$^{-/y}$ mice, circuit hyperexcitability can also be assessed by studying episodes of spontaneous activity, called UP states, in layer 4. UP states are generated by recurrent synaptic circuitry and resemble neurophysiological rhythms measured in vivo, such as during slow-wave sleep (55, 56). In *Fmr1*$^{-/y}$ mice, the duration of UP states is increased (54). To determine whether inhibition of GSK3α was also effective in reducing somatosensory cortical circuit excitability in *Fmr1*$^{-/y}$ mice, we prepared cortical slices from wild-type and *Fmr1*$^{-/y}$ mouse littermates and preincubated them for 1 hour in either DMSO vehicle or 25 μM BRD0705. Spontaneous UP states were recorded in layer 4 using extracellular multiunit recordings as described by Hays *et al.* (54). Consistent with previous reports, vehicle-treated *Fmr1*$^{-/y}$ slices displayed significantly longer UP states in comparison to vehicle-treated wild-type slices ($P = 0.001$). Inhibition of GSK3α with BRD0705 significantly reduced UP state duration in *Fmr1*$^{-/y}$ mouse cortical slices ($P = 0.0003$) but had no effect in wild-type mouse slices (Fig. 4, D and E). Together, the results suggest that inhibition of GSK3α was sufficient to correct hyperactivity across the sensory neocortex in *Fmr1*$^{-/y}$ mice.

BRD3731 inhibits GSK3β in vitro and in vivo

Unlike BRD0705, the GSK3β-selective compound BRD3731 was ineffective in ameliorating FXS phenotypes in the AGS assay in vivo (Fig. 1) and in the measures of cortical excitability and hippocampal protein synthesis in vitro (Figs. 2 to 4). To confirm that BRD3731 engaged the target and inhibited the action of GSK3β, we took advantage of a functional assay of synaptic plasticity, *N*-methyl-D-aspartate (NMDA) receptor (NMDAR)–dependent LTD. Previous studies have shown that a panel of compounds that inhibit GSK3 (SB415286, kenpaullone, lithium, CHIR99021, AR-164, and PenGSKi) all reliably inhibit LTD (57, 58). We found that the β-selective inhibitor BRD3731 applied to mouse hippocampal slices strongly inhibited LTD at the same 10 μM concentration that was ineffective in the *Fmr1*$^{-/y}$ protein synthesis and cortical excitability assays (Fig. 5A). Thus, the failure of BRD3731 to correct FXS phenotypes in brain slices was unlikely to be due to a failure to inhibit GSK3β.

We next asked whether dosing with BRD3731 in vivo enabled blockade of LTD in hippocampal slices. Animals received five consecutive doses of BRD3731 (30 mg/kg ip), which we had previously found to be ineffective in the AGS assay (fig. S5), and hippocampal slices were prepared 60 min after the last injection when the brain concentration of BRD3731 peaked (fig. S3). Even after removal of the brain and superfusion of the brain slices with artificial CSF (aCSF), the residual activity of the BRD3731 was sufficient to block NMDAR-dependent LTD (Fig. 5B). These findings confirm the pharmacokinetic study, showing that the compound entered the brain and engaged and inhibited GSK3β at doses that did not improve the AGS *Fmr1*$^{-/y}$ phenotype. This result stands in contrast to the effectiveness of the α-selective compound that, at comparable doses, ameliorated AGS in vivo (Fig. 1) and corrected both elevated protein synthesis and cortical hyperexcitability in vitro (Figs. 2 to 4).

To further verify that both the α- and β-selective compounds were penetrating the brain and inhibiting direct phosphorylation of GSK3 targets in vivo in a manner comparable to

lithium, we treated *Fmr1*$^{-/y}$ animals for five consecutive days with either vehicle, BRD3731 (30 mg/kg ip), BRD0705 (30 mg/kg ip), or lithium (60 mg/kg ip, twice daily). The right dorsal hippocampus was dissected 1 hour after the final dose, and phosphorylation of a well-described GSK3 substrate, T668 of amyloid precursor protein (APP) (59, 60), was assayed by Western blot analysis. This experiment confirmed reduced APP phosphorylation in vivo after treatment with either BRD0705, BRD3731, or lithium (Fig. 5C). All three drug treatments produced a comparable decrease in APP phosphorylation, suggesting that both GSK3α and GSK3β are capable of phosphorylating APP at this site. We also probed for changes in phosphorylation of T514 of CRMP2 but found that it was not changed by our positive control lithium or either experimental compound (fig. S8), suggesting that CRMP2 is not a useful marker for GSK3 inhibition in the hippocampus in vivo. Nevertheless, the observed inhibition of hippocampal APP phosphorylation and LTD confirmed that after in vivo dosing, BRD0705 and BRD3731 successfully entered the brain and inhibited the activity of GSK3α and GSK3β, respectively.

BRD0705 rescues performance in an inhibitory avoidance learning task

We next investigated the possibility that inhibition of GSK3α could reverse memory impairments in *Fmr1*$^{-/y}$ mice. We studied inhibitory avoidance memory because it is formed in a single trial, is impaired in *Fmr1*$^{-/y}$ mice, and is sensitive to manipulations of protein synthesis (48, 50, 61). In this task, mice learn the association of the dark side of a box with an aversive foot shock. Memory acquisition and subsequent extinction are assayed at several time points after conditioning by measuring the latency for mice to freely enter the dark side of the box when given the opportunity to do so. We administered BRD0705 (30 mg/kg) or vehicle intraperitoneally to adult wild-type or *Fmr1*$^{-/y}$ littermates for five consecutive days before conditioning with a foot shock (Fig. 6A). To minimize stress and behavioral modifications associated with the intraperitoneal injection itself, we administered “sham” saline injections once daily for 20 consecutive days before the first vehicle or BRD0705 injection. Consistent with previous findings, we observed that *Fmr1*$^{-/y}$ mice failed to form a strong association between the context (the dark side of the box) and the adverse outcome (foot shock) when measured 6 hours after training. However, *Fmr1*$^{-/y}$ mice chronically treated with BRD0705 exhibited normal memory acquisition and extinction over the course of 48 hours that was indistinguishable from either vehicle or BRD0705-treated wild-type mice (Fig. 6B).

BRD0705 does not augment MK-801–induced hyperlocomotion

It has been reported that first-generation mGluR5 NAMs have psychotomimetic effects in normal human volunteers (16–18). These adverse events are believed to be the result of the functional and physical interaction between mGluR5 and NMDARs (14, 62–70). The noncompetitive NMDAR blocker MK-801, which causes psychotomimetic effects in humans, induces hyperlocomotion in mice that is potentiated by pretreatment with mGluR5 NAMs (14, 15). To investigate whether a similar interaction occurs with BRD0705, we first confirmed that pretreatment with the selective mGluR5 inhibitor MTEP (3-[(2-methyl-1,3-thiazol-4-yl)ethynyl]-pyridine) (fig. S1) (71) potentiated MK-801–induced hyperlocomotion in wild-type mice (fig. S9). In marked contrast, we observed that pretreatment with BRD0705 had no effect on the behavioral response to MK-801. Thus, the data suggested

that inhibition of GSK3α could achieve the same therapeutic benefit as optimal inhibition of mGluR5 without dose limitations imposed by hyperlocomotion (presumably psychotomimetic) side effects.

Chronic administration of BRD0705 does not result in the development of tolerance

Another untoward effect of mGluR5 NAM treatment is the development of tolerance. Tachyphylaxis was initially suggested by Yan *et al.* (13), who showed that suppression of AGS in *Fmr1*$^{-/y}$ mice by the mGluR5 NAM MPEP (fig. S1) was greatly reduced after chronic dosing. Because durable efficacy was observed in some assays using the newer and more selective mGluR5 NAM CTEP [2-chloro-4-((2,5-dimethyl-1-(4-(trifluoromethoxy) phenyl)-1*H*-imidazol-4-yl)ethynyl) pyridine] (fig. S1) (48), we reexamined whether tolerance occurs in the AGS model using this compound. Although acute administration of CTEP (2 mg/kg, ip) significantly reduced the incidence of AGS in the *Fmr1*$^{-/y}$ mouse (P = 0.0038; fig. S10B), this protection was completely lost after three consecutive doses over 5 days (fig. S11A). To examine whether tolerance also developed with chronic exposure to BRD0705, we gave five doses of 30 mg/kg ip over 5 days. In contrast to what was observed with CTEP, there was no apparent loss of efficacy after repeated dosing with BRD0705 (fig. S11B). Amelioration of the seizure phenotype was comparable to what we observed with a single dose (Fig. 1C).

BRD0705 blocks mGluR-stimulated increases in protein synthesis and LTD downstream of ERK

Glutamate binding to mGluR5 has been shown to stimulate synaptic protein synthesis through activation of a signaling pathway that includes the small guanosine triphosphatase Ras and extracellular signal–regulated kinase 1/2 (ERK1/2). Hypersensitivity to stimulation of this pathway has been proposed to contribute to FXS symptoms (10, 51, 72). In support of this theory, it has been shown repeatedly that inhibitors of mGluR5, Ras, or MEK (mitogen-activated protein kinase kinase), the upstream regulator of ERK, all correct excessive protein synthesis and improve electrophysiological and behavioral phenotypes in *Fmr1*$^{-/y}$ mice (48–51, 73–77). We therefore wondered whether the therapeutic effects of BRD0705 were similarly a consequence of inhibiting the mGluR5-ERK1/2 pathway. To examine this question, we stimulated mGluR5 in hippocampal slices from both wild-type and *Fmr1*$^{-/y}$ mice using the orthosteric agonist DHPG (3,5-dihydroxyphenylglycine) and performed Western blot analysis of ERK1/2 phosphorylation (Fig. 7, A and B). To capture rapid changes in phosphorylation, slices were harvested after 5 min of DHPG exposure (51); to reduce variability and provide maximal activation, DHPG was applied after exposure to the selective mGluR5 positive allosteric modulator CDPPB [3-cyano-*N*-(1,3-diphenyl-1*H*-pyrazol-5-yl) benzamide]. The data showed comparable ERK1/2 phosphorylation after mGluR5 activation in vehicle and BRD0705-treated slices and, in agreement with previous findings (51), no difference between wild-type and *Fmr1*$^{-/y}$ mice. In addition, in agreement with previous results (51), no stimulation of the Akt-mTOR (mammalian target of rapamycin) pathway was observed after activation of mGluR5 in hippocampal slices from either genotype (fig. S12).

Although it is occluded by the elevated basal protein synthesis in *Fmr1*$^{-/y}$ slices, mGluR5-stimulated protein synthesis can be reliably detected using the metabolic labeling assay in hippocampal slices from wild-type mice (51). A number of treatments that prevent ERK1/2 pathway activation also block mGluR5-stimulated protein synthesis and the downstream functional consequences (51, 73, 78). Therefore, it was of particular interest to discover that BRD0705 was still effective in inhibiting protein synthesis stimulated by a 60-min treatment with CDPPB (Fig. 7, C and D). These data suggest that BRD0705 acts via a new mechanism, downstream of ERK1/2, to regulate FMRP-dependent protein synthesis.

One functional consequence of activating mGluR5 in the hippocampus is induction of an ERK- and protein synthesis–dependent form of hippocampal LTD (78, 79). We therefore additionally investigated the consequences of inhibiting GSK3α and GSK3β on LTD induced by brief DHPG treatment of hippocampal slices from both wild-type and *Fmr1*$^{-/y}$ mice (Fig. 8) (80). Consistent with our biochemistry results, we found that treatment of the slices with BRD0705, but not BRD3731, blocked stable expression of mGluR-LTD in slices from *Fmr1*$^{-/y}$ mice (Fig. 8A) and their wild-type littermates (Fig. 8B). Together, the data indicated that GSK3α, but not GSK3β, was required for the stimulation of protein synthesis downstream of mGluR5.

DISCUSSION

The results of our experiments indicated that selective inhibition of GSK3α was sufficient to ameliorate several phenotypes in the *Fmr1*$^{-y}$ mouse model of FXS. Among the phenotypes corrected were excessive basal protein synthesis in hippocampus, increased electrical excitability in sensory neocortex, increased susceptibility to AGS, and impaired inhibitory avoidance memory. The extent of this phenotypic rescue was comparable to what has been observed by inhibiting mGluR5 (13, 48, 50) and the downstream ERK1/2 signaling cascade (49, 51, 73, 77). However, unlike the mGluR5 NAMs, inhibition of GSK3α with BRD0705 did not reduce ERK1/2 pathway activation, augment the psychotomimetic effects of MK-801, or exhibit tachyphylaxis with repeated dosing. Thus, selective inhibitors of GSK3α may be differentiated from mGluR5 NAMs, which thus far have failed in FXS clinical trials.

Our findings with BRD0705 are generally consistent with what has been observed using lithium treatment in *Fmr1*$^{-/y}$ mice (20, 22, 23, 81–83). Along with the correction of excessive cerebral protein synthesis in vivo, lithium improves a number of electrophysiological and behavioral phenotypes without development of tolerance. The hypothesis that the therapeutic actions of lithium are due to GSK3 inhibition (27) has been supported by experiments using more potent small-molecule inhibitors including CHI99021, SB415286, TDZD-8, and VP0.7. However, all of these compounds directly inhibit both paralogs of GSK3. While dual GSK3α/β inhibitors have entered clinical trials, none has successfully translated to clinical application due to mechanism-based toxicities, driven in part by β-catenin stabilization.

The hypothesis that hyperactive GSK3 contributes to FXS pathophysiology derives in part from the finding of decreased inhibitory phosphorylation of both α and β paralogs in the

Fmr1$^{-/y}$ mouse (19, 20, 83, 84). One study showed that GSK3α, but not GSK3β, is overactive in the *Fmr1*$^{-/y}$ mouse hippocampus (19), and we have confirmed this finding. The development of GSK3 inhibitors with about 10-fold paralog selectivity (33, 47) has now given us the opportunity to examine the relative contribution of GSK3α and GSK3β to aspects of FXS pathophysiology. Evidence collected in the present series of experiments suggests that inhibition of GSK3α provides therapeutic benefit in the *Fmr1*$^{-/y}$ mouse. These findings suggest that phenotypic improvements with lithium or other nonspecific pan-GSK3 inhibitors may have been misattributed to inhibition of only GSK3β in previous studies (23, 81, 85). We found that chronic in vivo exposure to the β-selective inhibitor BRD3731 failed to improve the AGS phenotype in *Fmr1*$^{-/y}$ mice despite producing strong inhibition of NMDAR-dependent LTD, a sensitive functional measure of enzyme activity (57, 58). Acute application in vitro of BRD3731 to brain slices from *Fmr1*$^{-/y}$ mice also failed to correct excessive hippocampal protein synthesis or sensory cortex hyperexcitability, unlike what was observed with BRD0705. The contrasting effects of BRD3731 and BRD0705 on NMDAR- and mGluR5-dependent forms of LTD provide additional support for the conclusion that the α paralog of GSK3 is of particular importance for the regulation of protein synthesis that is aberrant in FXS.

There are several limitations to the present study, the foremost of which is that we cannot rule out the possibility that stronger inhibition of GSK3β with higher doses of BRD3731 may be effective in the *Fmr1*$^{-/y}$ mice. In addition, an argument could be made that the effects of BRD0705 are mediated by inhibition of a target other than GSK3α, possibly including GSK3β. We note that another group has reported improvement in FXS phenotypes with intranasal small interfering RNA (siRNA) directed against the GSK3β paralog, but they did not measure and were careful not to exclude the possibility that the treatment reduced GSK3α (86). Validation of the selectivity of our treatments would be aided by identification of paralog-selective GSK3 substrates in vivo, which so far has been challenging (87) and will require further phosphoproteomic analysis. We did probe for changes in the phosphorylation of the FXS-relevant GSK3 substrate APP (88) after treatment in vivo with either lithium (nonselective), BRD0705 (α-selective), or BRD3731 (β-selective). Exposure to all three treatments produced comparable inhibition, suggesting that APP phosphorylation by GSK3 was not paralog selective (Fig. 5C). However, the distinguishing feature of the therapeutically effective treatments (lithium and BRD0705) is inhibition of the α paralog, which presumably contributes to FXS pathogenesis by phosphorylation of a substrate other than APP. Although it is impossible to rule out unknown actions of a drug, BRD0705 is notable for its exquisite kinome selectivity (33). The reported cellular IC_{50} in human embryonic kidney (HEK) cells for BRD0705 of 4.8 μM against GSK3α and >20 μM against GSK3β (47) supports the conclusion that at the doses used in this study, the treatment is selective for GSK3α.

The current results suggest that selective inhibition of GSK3α is sufficient to correct an array of *Fmr1*$^{-/y}$ phenotypes. This finding is important, as a major toxicity that arises from inhibition of GSK3—increased β-catenin—fails to occur with paralog-selective inhibition (33, 47) or haploinsufficiency (46). Although inhibition of GSK3 by lithium apparently is weak enough to avoid β-catenin–mediated toxicity, lithium is of limited usefulness for treatment of children with FXS due to other well-known side effects (presumably unrelated

to GSK3), including nausea, tremor, fatigue, enuresis, irritability, and impaired renal and thyroid functions (29). Selective inhibition of GSK3α, therefore, has the potential to confer benefit in FXS without some of the side effects that have limited treatment with lithium or the first-generation mGluR5 NAMs. Unlike the GSK3β-null mouse, the GSK3α knockout mouse is viable (44, 45). Of course, the safety of chronic inhibition of GSK3α will need to be fully evaluated in extensive preclinical studies before contemplating prolonged treatment in human patients. Our finding that treatment with BRD0705 failed to potentiate MK-801–induced hyperactivity is encouraging and suggests that it will not have the same psychotomimetic effects as the mGluR5 NAMs, but clearly much more study is required to assess other potential side effects.

Precisely where GSK3α fits into the intracellular pathways that give rise to FXS phenotypes remains to be determined. In wild-type mice, BRD0705 had no effect on basal protein synthesis or synaptic transmission, but it did block stimulated protein synthesis and LTD induced by activation of mGluR5. Under our experimental conditions, previous studies have shown that ERK1/2 is obligatory for mGluR5-stimulated mRNA translation and LTD in the hippocampus and that inhibition of this pathway corrects excessive protein synthesis in *Fmr1*$^{-/y}$ mice (51). Here, we have found that inhibiting GSK3α similarly corrects protein synthesis in the mutant mice but did not affect mGluR5-dependent ERK1/2 activation. These data suggest that GSK3α may lie downstream of ERK1/2 in the pathway that links mGluR5 to initiation of protein synthesis. Serine-21 of GSK3α, hypophosphorylated in *Fmr1*$^{-/y}$ mice (19, 20, 83), is a substrate of the protein kinases Akt and protein kinase A (PKA) (89). There is evidence that both Akt (53, 90) and PKA (91) signaling are impaired in FXS animal models. Thus, it is possible that GSK3α is a hub or convergence point for several signaling pathways that contribute to FXS pathophysiology. In any case, decreased phosphorylation of some GSK3α substrate proteins presumably is responsible for the therapeutic effect of BRD0705, and phosphoproteomic studies will be required to elucidate what these are.

The phenotype of elevated bulk protein synthesis in acutely prepared hippocampal slices has been widely reproduced in multiple laboratories and animal models of FXS (50, 51, 77, 92) and is consistent with observations in *Fmr1*$^{-/y}$ mice in vivo (23, 52, 93), as well as in cultured neurons from *Fmr1*$^{-/y}$ mice and patient-derived fibroblasts (94). Because FMRP functions normally as a translational repressor (95), it has been proposed that increased constitutive protein synthesis may be a proximal cause of other diverse FXS phenotypes (6, 96). Treatments that acutely correct this biochemical phenotype in brain slices, including (but not limited to) inhibitors of mGluR5 (13, 48, 50), Ras (49, 97), and ERK1/2 (51, 77), all produce a broad rescue of other FXS phenotypes at the synaptic, cellular, and behavioral levels. However, recent findings suggest that the measured increases in bulk protein synthesis are not necessarily a direct consequence of the loss of translational repression by FMRP. For example, it was found that the transcripts overrepresented on translating ribosomes in hippocampal slices from *Fmr1*$^{-/y}$ mice are not FMRP targets (98) and, further, that the biochemical and synaptic phenotypes related to protein synthesis in slices are altered substantially when the aCSF is supplemented with essential amino acids (99). Thus, it cannot be assumed that elevated bulk protein synthesis and protein synthesis–dependent LTD measured under conditions that are standard for brain slice electrophysiology are root causes of other disease phenotypes. These new revelations do not alter our conclusion that

inhibition of GSK3α is broadly effective in correcting FXS phenotypes in *Fmr1*$^{-/y}$ mice at multiple levels of analysis or the conclusion that previous findings with lithium (including correction of the FXS protein synthesis phenotype in vivo) (23) are likely due to inhibition of the α paralog of GSK3. However, they do need to be taken into consideration in the search for the mechanism of therapeutic benefit.

FXS has offered one of the first opportunities to fulfill the promise of molecular medicine in a complex neuropsychiatric disease: progressing from gene identification to studies of pathophysiology in genetically validated animal models to therapeutic target identification and, ultimately, to clinical trials (9). Studies in animal models of FXS (flies, fish, mice, and rats) have shown that disease modification is possible, even after the onset of symptoms (6, 8). The challenges of translation from animal models to human therapeutics are well known, however, and FXS has proven to be no exception. Careful clinical studies in this disease are still in their infancy, and the work to date has been more valuable for identifying key variables in trial design (e.g., patient selection, treatment dose, duration, age of onset, and appropriate clinical end points) than for testing the theory that disease modification is possible in humans by targeting core pathophysiological processes, such as altered cerebral protein synthesis. Nevertheless, the outcomes of two clinical studies using 12 weeks of treatment with the mGluR5 NAM mavoglurant (age ranges 12 to 17 and 18 to 45, respectively) were still disappointing (12), leading some to question the applicability of the animal findings to humans (100). This skepticism will persist until an unequivocal success is observed in a well-controlled human study. In the meantime, the clinical findings to date have forced a re-examination of the limitations of first-generation mGluR5 NAMs, which are now understood to include psychiatric side effects that limit dose selection and the possible development of tolerance with chronic exposure. The results presented here suggest that it is feasible to correct core FXS phenotypes by inhibiting GSK3α without tachyphylaxis or psychotomimetic effects. Furthermore, we know from human clinical experience with lithium that modest inhibition of GSK3 can be therapeutic without causing β-catenin–induced toxicity. Paralog-selective inhibition of GSK3α circumvents limitations imposed by off-target actions of lithium and provides a new treatment modality for the pathophysiology of FXS.

MATERIALS AND METHODS

Study design

Attempts to apply GSK3 inhibitors for therapeutic use have been plagued by various toxicities, driven in part by the simultaneous inhibition of both GSK3 paralogs. The development of GSK3 inhibitors with about 10-fold paralog selectivity (33, 47) provided the opportunity to examine the relative contribution of GSK3α and GSK3β to aspects of FXS pathophysiology. In this study, we used the paralog-specific inhibitors BRD0705 and BRD3731 of GSK3α and GSK3β, respectively. We dosed *Fmr1*$^{-/y}$ mice and their wild-type littermates in vivo and treated mouse brain slices with the compounds ex vivo. The action of GSK3α and GSK3β inhibitors was assayed on a variety of *Fmr1*$^{-/y}$ mouse phenotypes including hippocampal protein synthesis, susceptibility to AGS, sensory cortex hyperexcitability, mGluR5- and protein synthesis–dependent LTD, and deficits in learning

and memory. Sample size was determined via a power analysis or laboratory convention; no outliers were removed from any data sets. Animals were chosen at random for treatment and, where applicable, a balanced number of *Fmr1*$^{-/y}$ mice and their wild-type littermates were used. *Fmr1*$^{-/x}$ female mice (the Jackson Laboratory) were crossed with wild-type C57BL/6J male mice to generate wild-type and *Fmr1*$^{-/y}$ male offspring. All experimental animals were age-matched littermates and were studied with the experimenter blind to genotype and treatment condition. Animals were group-housed on static racks and maintained on a 12-hour light/12-hour dark cycle. The Institutional Animal Care and Use Committee at Massachusetts Institute of Technology (MIT) and University of Texas (UT) Southwestern approved all experimental techniques, and all animals were treated in accordance with the National Institutes of Health (NIH), MIT, and UT Southwestern guidelines.

Reagents

GSK3 inhibitors BRD0320, BRD3731, and BRD0705 (47) were all synthesized at the Broad Institute. All final compounds were confirmed to be of ≥95% purity on the basis of HPLC (high-performance liquid chromatography), LC-MS (liquid chromatography–mass spectrometry), and ^{1}H NMR (proton nuclear magnetic resonance) analyses. The reported biochemical IC_{50} values for BRD3731 are 0.215 μM against GSK3α and 0.015 μM against GSK3β and those for BRD0705 are 0.066 against GSK3α and 0.515 against GSK3β. The reported cellular EC_{50} (half-maximal effective concentration) values in HEK293 cells for BRD3731 are >20 μM against GSK3α and 3.3 μM against GSK3β, and those for BRD0705 are 4.8 μM against GSK3α and >20 μM against GSK3β (47). This enzyme-to-cellular assay potency shift is consistent with the literature for kinase inhibitors and, at these concentrations in cell-based assays, selectivity is still maintained (47). Critically, the cell-based assay concentrations are on par with the achieved in vivo exposure at the effective doses. For these reasons, isoform-selective inhibition is expected at these doses in vivo.

All compounds for acute and chronic AGS, inhibitory avoidance, and MK-801–induced hyperlocomotion were administered at a dose of 30 mg/kg in a vehicle of 10% DMSO, 45% PEG 400, and 45% normal saline. For chronic AGS and inhibitory avoidance, vehicle and drug were delivered intraperitoneally at a dosing volume of 10 ml/kg. For MK-801–induced hyperlocomotion, vehicle and drug were delivered intraperitoneally at a dosing volume of 2 ml/kg with a needle with precision for small volumes, used because of gastrointestinal complications and impact on locomotion at higher doses of the DMSO and PEG 400 vehicle. For slice experiments, all GSK3 inhibitors were prepared as 50 mM stocks in DMSO and stored in aliquots at −20°C. (*S*)-3,5-dihydroxyphenylglycine (S-DHPG) was purchased from Tocris Bioscience. Fresh bottles of DHPG were prepared as a 100× stock in H_2O, divided into aliquots, and stored at −80°C. Fresh stocks were made once a week. Actinomycin D (Tocris Bioscience) was prepared as a stock solution of 1 mg/ml in 0.01% DMSO and aCSF and stored at −20°C. CDPPB (Tocris Bioscience) was prepared daily at 75 mM stock in DMSO. MK-801 (Sigma-Aldrich) was prepared in H_2O daily, and 0.3 mg/kg was injected intraperitoneally at a dosing volume of 10 ml/kg. MTEP (Tocris Bioscience) was prepared in H_2O daily, and 10 mg/kg was injected intraperitoneally at a dosing volume of 10 ml/kg. CTEP was formulated as a microsuspension in vehicle (0.9% NaCl and 0.3%

Tween 80). Chronic treatment consisted of one dose every 48 hours at 2 mg/kg (ip) in a volume of 10 ml/kg.

Pharmacokinetics

All pharmacokinetics studies were conducted at Sai Life Sciences Limited, Pune, India, in accordance with the guidelines provided by the Committee for the Purpose of Control and Supervision of Experiments on Animals as published in *The Gazette of India*, 15 December 1998. Prior approval of the Institutional Animal Ethics Committee was obtained before initiation of the studies. The objective of this study was to investigate the plasma and CSF pharmacokinetics and brain distribution of each of the BRD compounds in male C57BL/6 mice after a single intraperitoneal dose administration. For each study, a group of 14 male mice were administered intraperitoneally with the BRD compound solution formulation in 10% DMSO and 45% PEG 400 in normal saline at 30 mg/kg dose. Blood samples (approximately 60 μl) were collected from retro orbital plexus under light isoflurane anesthesia such that the samples were obtained at 0.08, 0.5, 1, 2, 4, 8, and 24 hours. The blood samples were collected from a set of three mice at each time point in a labeled microcentrifuge tube containing K2-EDTA as anticoagulant. Plasma samples were separated by centrifugation of whole blood and stored below −70°C until bioanalysis. After collection of blood, CSF and brain samples were collected at 0.08, 0.5, 1, 2, 4, 8, and 24 hours. Collected brains were dipped in 20 ml of fresh phosphate-buffered saline (pH 7.4) buffer three times, dried on blotted paper, and weighed. Brain samples were homogenized using ice-cold phosphate-buffered saline (pH 7.4), and homogenates were stored below −70°C until analysis. Total homogenate volume was three times the brain weight. All samples were processed for analysis by protein precipitation using acetonitrile and analyzed with a fit-for-purpose LC/MS/MS method [lower limit of quantitation (LLOQ): 1.02 ng/ml]. Pharmacokinetic parameters were calculated using the noncompartmental analysis tool of Phoenix WinNonlin (version 6.3).

AGS assay

AGS experiments were performed as previously described (50). Mice were housed on static racks to prevent auditory desensitization that occurs with chronic exposure to the ambient noise of ventilated racks. For acute dosing, animals were injected with either vehicle or drug 1 to 2 hours before exposure to the alarm in a separate room. For chronic dosing, animals were injected for four consecutive days before testing with BRD0705 or BRD3731 and received a final (fifth) injection 1 to 2 hours before testing. Animals chronically dosed with CTEP were given three doses, one every 48 hours, with the final dose occurring 1 to 2 hours before testing. All animals were run at postnatal day 23 (P23) to P25 (immediately after weaning) and were habituated to the behavioral chamber (28 cm by 17.5 cm by 12 cm transparent plastic box) for 1 min before stimulus onset. AGS stimulus was a 125-dB at 0.25-m siren (modified personal alarm, RadioShack model 49–1010, powered from a DC converter). Seizures were scored for incidence during a 2-min stimulus presentation or until animal reached AGS end point (wild running/jumping, status epilepticus, respiratory arrest, or death were all scored as seizure activity).

Metabolic labeling

Metabolic labeling of new protein synthesis was performed as previously described (51). Male P28 to P32 littermate mice were anesthetized with isoflurane, and the hippocampus was rapidly dissected into ice-cold aCSF (124 mM NaCl, 3 mM KCl, 1.25 mM NaH_2PO_4, 26 mM $NaHCO_3$, 10 mM dextrose, 1 mM $MgCl_2$, and 2 mM $CaCl_2$, saturated with 95% O_2 and 5% CO_2). Hippocampal slices (500 μm) were prepared using a Stoelting Tissue Slicer and transferred into 32.5°C aCSF (saturated with 95% O_2 and 5% CO_2) within 5 min. Slices were incubated in aCSF undisturbed for 3 hours to allow recovery of basal protein synthesis and then transferred to either aCSF containing vehicle (DMSO) or drug, which was present for the remainder of the experiment. Actinomycin D (25 μM) was then added to the chamber for 30 min to inhibit transcription, after which slices were transferred to fresh aCSF containing [^{35}S] Met/Cys (~10 mCi/ml; PerkinElmer) for an additional 30 min. Slices were then homogenized, and labeled proteins were isolated by trichloroacetic acid precipitation. Samples were read with a scintillation counter and subjected to a protein concentration assay (Bio-Rad). Data were analyzed as counts per minute per microgram of protein, normalized to the [^{35}S] Met/Cys aCSF used for incubation, and the average incorporation of all samples was analyzed and then normalized to percent wild type for each experiment. Statistical significance was determined using a two-way analysis of variance (ANOVA) for genotype and treatment. For experiments in which wild-type slices were stimulated with CDPPB, four slices from each animal were prepared with the method described above, and each slice was randomly placed in one of four recovery chambers, following the protocol described above. After 2.5 hours of recovery, 10 μM BRD0705 or vehicle was added to the bath of two chambers each (and remained in the bath for the remainder of the experiment). After 30 min, 10 μM CDPPB or vehicle was added to one chamber containing drug and one chamber containing vehicle for 30 min. Metabolic labeling and slice processing were performed as described above. Statistical significance was determined using within-subject two-way ANOVA (treatment × stimulation) where treatment is the within-subject variable.

Evoked and spontaneous spiking in mouse visual cortex

Slices of visual cortex were prepared from P16 to P21 wild-type or *Fmr1*$^{-/y}$ male animals. Slices (350 μm) were prepared using a Leica vibratome in ice-cold cutting solution containing 87 mM NaCl, 3 mM KCl, 1.25 mM NaH_2PO_4, 26 mM $NaHCO_3$, 0.5 mM $CaCl_2$, 7 mM $MgCl_2$, 20 mM glucose, 1.3 mM ascorbate, and 75 mM sucrose, saturated with 95% O_2 and 5% CO_2. Slices were recovered for 30 min at 32°C and then for an additional 2.5 hours at room temperature in a modified aCSF containing 124 mM NaCl, 3.5 mM KCl, 1.25 mM NaH_2PO_4, 26 mM $NaHCO_3$, 10 mM glucose, 0.8 mM $MgCl_2$, and 1 mM $CaCl_2$, saturated with 95% O_2 and 5% CO_2. Action potentials were evoked by electrical stimulation of the white matter (clustered bipolar tungsten, FHC) and recorded by placing a glass recording electrode (~1-megohm resistance when filled with aCSF) in layer 5 of the visual cortex. A single, 0.2-ms-duration, electrical stimulation was delivered every 30 s using a stimulus intensity between 35 and 80 μA. Evoked and spontaneous extracellular recordings were first collected in vehicle conditions for 30 min (60 trials total), followed by 30 additional minutes in the presence of either 10 μM BRD0705 or 10 μM BRD3731. All recordings were made using a Multiclamp 700B amplifier (Molecular Devices), amplified 1000 times, filtered between 300 Hz and 10 kHz, and digitized at 25 kHz. Evoked events

were those measured for the first 3.2 s after electrical stimulation of the white matter. Spontaneous events were classified as those occurring between 3.2 and 30 s after stimulation.

UP state recordings

Spontaneous UP states were recorded at the UT Southwestern from acute slices of somatosensory, barrel cortex prepared from P19 to P23 wild-type or *Fmr1* KO male littermates on the C57bl6CR background as previously described (54, 90, 101). Mice were anesthetized with ketamine (120 mg/kg) and xylazine (25 mg/kg) and decapitated. The brain was transferred into ice-cold dissection buffer containing 87 mM NaCl, 3 mM KCl, 1.25 mM NaH_2PO_4, 26 mM $NaHCO_3$, MgSO4, 7 mM $MgCl_2$, 0.5 mM $CaCl_2$, 20 mM D-glucose, 75 mM sucrose, and 1.3 mM ascorbic acid saturated with 95% O_2 and 5% CO_2. Thalamocortical slices (400 μm) were made on an angled block (102) using a Leica vibratome. After cutting, slices were transected parallel to the pia mater to remove the thalamus and midbrain. Slices were immediately transferred to an interface recording chamber (Harvard Instruments) and allowed to recover for 1 hour in aCSF at 32°C containing 126 mM NaCl, 3 mM KCl, 1.25 mM NaH_2PO_4, 26 mM $NaHCO_3$, 2 mM $MgSO_4$, 2 mM $CaCl_2$, and 25 mM D-glucose at 29° to 30°C.

Slices were then transferred to an aCSF that mimics physiological ionic concentrations in vivo (56, 103), containing 126 mM NaCl, 5 mM KCl, 1.25 mM NaH_2PO_4, 26 mM $NaHCO_3$, 2 mM $MgSO_4$, 1 mM $CaCl_2$, and 25 mM D-glucose. This aCSF also contained BRD0705 or DMSO vehicle (25 μM; 0.1% DMSO). After 1-hour preincubation in compound or vehicle, spontaneous UP states were recorded using 0.5-megohm tungsten microelectrodes (FHC) placed in layer 4 of the somatosensory cortex. Ten minutes of spontaneous activity was collected from each slice. Recordings were amplified 10,000-fold and filtered online between 500 Hz and 3 kHz. All measurements were analyzed offline using custom LabVIEW software. Traces were rectified and band-pass–filtered at 0.2 Hz. The threshold for detection was set at 5× the root mean square noise. An event was defined as an UP state if its amplitude remained above the threshold for at least 200 ms. The end of the UP state was determined when the amplitude decreased below threshold for >600 ms. Two events occurring within 600 ms of one another were grouped as a single UP state. To determine effects of drug on UP state duration in wild-type and $Fmr1^{-/y}$ mice, a two-way ANOVA and post hoc Sidak's multiple comparisons were performed.

Hippocampal LTD measurements

Hippocampal slices were prepared from P21 to P35 male C57/B6 mice (Charles River Laboratories). Each animal was anesthetized with isoflurane vapor and decapitated. The brain was rapidly removed and immersed in ice-cold dissection buffer (composition: sucrose, 75 mM; KCl, 2.5 mM; NaH_2PO_4, 1.25 mM; $NaHCO_3$, 25 mM; dextrose, 10 mM; $MgCl_2$,7 mM; and $CaCl_2$, 0.5 mM) bubbled with 95% O_2 and 5% CO_2. A block of hippocampus was removed and sectioned in the transverse plane into 350-μm-thick slices with a vibratome. The slices were gently transferred to a holding chamber containing aCSF (composition: NaCl, 124 mM; KCl, 3 mM; NaH_2PO_4, 1.25 mM; $NaHCO_3$, 26 mM; dextrose, 10 mM; $MgCl_2$, 1 mM; and $CaCl_2$, 2 mM) bubbled with 95% O_2 and 5% CO_2.

The slices were left in the holding chamber at 32°C for 60 min to recover. For the mGluR-dependent LTD experiments, slices were allowed a further 120 min of recovery time at room temperature to allow for recovery of protein synthesis (51). Slices were then gently transferred to a submersion-type recording chamber continually perfused with 28°C oxygenated aCSF at a rate of 2 ml/min. Slices were left undisturbed in the recording chamber for ≥20 min before recording. Synaptic responses were measured extracellularly in the stratum radiatum of CA1 using glass microelectrodes (borosilicate: outer diameter, 1.0 mm; inner diameter, 0.78 mm; Sutter Instrument, Novato, CA) filled with aCSF (1 to 2 megohms). Baseline responses were evoked by stimulation (20 to 50 μA) of the Schaffer collaterals once every 30 s with a two-contact cluster electrode (FHC) using a 0.2-ms stimulus yielding 40 to 60% of the maximal response. Field excitatory postsynaptic potential (fEPSP) recordings were filtered at 0.1 Hz to 1 kHz, amplified 1000 times, digitized at 10 kHz, and analyzed using pCLAMP 9 (Axon Instruments). The initial slope of the response was used to assess changes in synaptic strength. Data were normalized to the baseline response and are presented as group means ± SEM. The input-output function was examined by stimulating slices with incrementally increasing current and recording the fEPSP response. Homosynaptic NMDAR-dependent LTD was induced by delivering low-frequency stimulation (LFS; 900 pulses at 3 Hz) at the same stimulation intensity as baseline (104). mGluR-dependent LTD was induced by application of DHPG (100 μM, 5 min) (80).

Inhibitory avoidance assay

Inhibitory avoidance experiments were performed as previously described (50). On the day of testing, P56 to P76 animals were placed into the dark compartment of an inhibitory avoidance training box (a two-chambered Perspex box consisting of a lighted safe side and a dark shock side separated by a trap door) for 30 s followed by 90 s in the light compartment for habituation. After the habituation period, the door separating the two compartments was opened and animals were allowed to enter the dark compartment. Latency to enter after door opening was recorded (“baseline”, time 0, 8:00 to 9:00 a.m.); animals with baseline entrance latencies of greater than 120 s were excluded. After each animal stepped completely into the dark compartment with all four paws, the sliding door was closed and the animal received a single scrambled foot shock (0.5 mA, 2.0 s) via electrified steel rods in the floor of the box. This intensity and duration of shock consistently caused animals to vocalize and jump. Animals remained in the dark compartment for 15 s after the shock and were then returned to their home cages. Six to seven hours after inhibitory avoidance training, mice received a retention test (“post-acquisition”, time 6 hours, 2:00 to 3:00 p.m.). During post-acquisition retention testing, each animal was placed in the lit compartment as in training; after a 90-s delay, the door opened, and the latency to enter the dark compartment was recorded (cutoff time, 537 s). For inhibitory avoidance extinction training, animals were allowed to explore the dark compartment of the box for 200 s in the absence of foot shock (animals remaining in the lit compartment after the cutoff were gently guided, using an index card, into the dark compartment); after inhibitory avoidance extinction training, animals were returned to their home cages. Twenty-four hours after initial inhibitory avoidance training, mice received a second retention test (“post-extinction 1”, time 24 hours, 8:00 to 9:00 a.m.). Animals were tested in the same way as at the 6-hour time point, followed by a second 200-s extinction trial in the dark side of the box; after training, animals were again returned to their home

cages. Forty-eight hours after avoidance training, mice received a third and final retention test (“post-extinction 2”, time 48 hours, 8:00 to 9:00 a.m.).

MK-801–induced hyperlocomotion measurements

To determine the effects of genotype on MK-801–induced hyperlocomotion, mice were habituated in the open field (40 cm by 40 cm by 40 cm box) for 60 min, followed by the administration of vehicle or MK-801, and locomotor activity was recorded for another 60 min. To determine the effects of MTEP and BRD0705 on MK-801–induced hyperlocomotion, mice were habituated in the open field for 30 min, followed by the intraperitoneal administration of MTEP (10 mg/kg at a dosing volume of 10 ml/kg) or BRD0705 (30 mg/kg at a dosing volume of 2 ml/kg). After an additional 30 min, MK-801 (0.3 mg/kg at a dosing volume of 10 ml/kg) was administered intraperitoneally, and locomotor activity was recorded for another 60 min. The time course of drug-induced changes in ambulation was expressed as centimeters traveled per 5 min over the 120-min session. Sessions were recorded using Plexon’s CinePlex Studio and analyzed using Plexon’s CinePlex Editor and code was written in MATLAB. MK-801–induced locomotor activity was scored and analyzed using the average of the final 5 min (minutes 115 to 120) of observation per cohort.

Immunoblotting

For assessment of ERK pathway activation after mGluR5 stimulation, hippocampal slices were prepared and recovered as described in metabolic labeling experiments. Sets of slices from each animal were treated with the mGluR5 positive allosteric modulator CDPPB (10 μM) for 30 min followed by the agonist DHPG (50 μM) for 5 min and then flash-frozen in liquid nitrogen immediately after stimulation, before processing. Yoked unstimulated slices from the same animal were also processed to assess basal signaling. Immunoblotting was performed according to established methods using primary antibodies to p-ERK1/2 (Thr^{202}/Tyr^{204}) (Cell Signaling Technology), ERK1/2 (Cell Signaling Technology), p-Akt (Ser^{473}) (Cell Signaling Technology), Akt (Cell Signaling Technology), p-S6 240/44 (Cell Signaling Technology), and S6 (Cell Signaling Technology). Protein quantification was performed by measuring densitometry (Quantity One) and quantified as the densitometric signal of phospho-protein divided by the total protein signal in the same lane.

For analysis of GSK3 substrate phosphorylation in vivo, immediately after euthanization, the head was rapidly cooled in liquid nitrogen (105, 106) and the right dorsal hippocampus was removed and then immediately flash-frozen in liquid nitrogen. Lysate was run on an SDS–polyacrylamide gel electrophoresis (PAGE) gel (4 to 20% gradient, Bio-Rad), followed by nitrocellulose membrane transfer. Membranes were incubated overnight with primary antibodies in a solution of tris-buffered saline containing Tween 20 (TBST, Sigma-Aldrich) and 5% dry milk. Incubation of secondary antibodies was performed for 1 hour at room temperature in a solution of 5% dry milk in TBST. Immunoblot staining was developed using ECL (GE healthcare), digitally captured using Bio-Rad ChemiDoc MP Imaging System, and analyzed using Image Lab v6.0.1 (Bio-Rad). Immunoblotting was performed according to established methods using primary antibodies to p-CRMP2 (T514) (Cell Signaling Technology #9397), CRMP total (Cell Signaling Technology #9393), p-APP T668

(Cell Signaling Technology #3823), and APP Y188 (Abcam #32136). Protein bands were measured by densitometry and quantified as the densitometric signal of phospho-protein band divided by the total protein band. Total protein signal was divided by the densitometric signal of the Pierce reversible protein stain (Thermo Fisher Scientific) for the lane as loading control.

To probe phosphorylation and expression of Wnt signaling proteins and GSK3α/β paralogs, SH-SY5Y cultured cells treated with various compounds were collected in ice-cold lysis buffer with protease and phosphatase inhibitors as described previously (107). The samples were incubated and gently rocked for 1 hour before centrifuged at 12,000*g* for 10 min (both at 4°C). The supernatant total cell lysate was subjected to subsequent Western blot analysis. Lysate was run on an SDS-PAGE gel (4 to 12% gradient, Bio-Rad), followed by polyvinylidene difluoride (PVDF) membrane transfer to analyze the whole-cell lysate. Membranes were incubated overnight with primary antibodies in a solution of TBST (Sigma-Aldrich) and 5% dry milk. Incubation of secondary antibodies was performed for 1 hour at room temperature in a solution of 5% dry milk in TBST. Immunoblot staining was developed using femto peroxidase substrate (Thermo Fisher Scientific), digitally captured using Bio-Rad ChemiDoc MP imaging system, and analyzed using ImageJ software (NIH). The following antibodies were used: p-catenin (S33/37/T41, Cell Signaling Technology, 9561), β-catenin total (Cell Signaling Technology, 9562), p-CRMP (T514) (Cell Signaling Technology, 9397), CRMP total (Cell Signaling Technology, 9393), pGSK3α/β (S21/S9) (Cell Signaling Technology, 9331), pGSK3α/β (Y279/216) (Thermo Fisher Scientific, OPA-03083), and GSK3 α/β (Cell Signaling Technology, 5676S).

Statistical analysis

All experiments were performed blind to genotype and drug treatment and included same-day controls for genotype and drug treatment. All data are expressed as mean ± SEM, with *n* values represented in the figures and figure legends. Unless indicated otherwise, the *n* values stated in figures and figure legends represent numbers of animals (in experiments in which more than one measurement was taken from an animal, the value representing this animal is the average of technical replicates). For the cell culture–based experiments in fig. S2, the *N* represents individual replicates. The effects of compound treatment on β-catenin and p-CRMP2 were determined using a Dunnett's multiple comparison test. Differences in AGS incidence were determined using a two-tailed Fisher's exact test. For brain slice electrophysiology experiments, the effects of genotype and drug treatment were determined using either a two-way repeated measures ANOVA with Bonferroni's post hoc analysis (for spiking experiments) or a two-way ANOVA with Sidak's multiple comparisons (for UP states). The effect of BRD0705 or BRD3731 acute treatment on mouse brain slices was determined using a paired two-tailed Student's *t* test. For protein synthesis in Fig. 2, differences between genotype and drug treatment were determined using a two-way ANOVA with two-tailed Student's *t* test for post hoc analysis. For protein synthesis in Fig. 7, differences between genotype and drug stimulation conditions were determined using a two-way repeated measures ANOVA. For Western blotting experiments in Fig. 7 and fig. S11, differences between genotype, drug, and stimulation were determined using a three-way ANOVA with Dunnett's multiple comparisons test. Differences between genotypes and

treatment in the inhibitory avoidance assay were determined using a repeated measures three-way ANOVA with Greenhouse-Geisser correction. The effects of treatment on hyperlocomotion were determined using ANOVA on ranks test with Holm-Sidak pairwise multiple comparisons and Student's *t* tests used for post hoc analysis. For LTD electrophysiology experiments, the effects of drug treatment were determined by a one-way ANOVA with Bonferroni's post hoc analysis.

Supplementary Material

Refer to Web version on PubMed Central for supplementary material.

Acknowledgments:

We thank A. Coronado, E. Hickey, and K. Chu for technical assistance. We are also pleased to acknowledge S. Meagher, N. Palisano, and J. Buckey for administrative assistance.

Funding:

This research was supported in part by grants to M.F.B. from NIMH (R01MH106469), the Simons Foundation (SFARI #240559), the JPB Foundation, and the Stanley Center for Psychiatric Research. K.M.H. and V.S. were supported by a grant from the NIH (U54 HD82008). L.J.S. received support from grant #T32MH074249. P.K.M. and R.K.S. were supported in part by grants from FRAXA Research Foundation.

REFERENCES AND NOTES

1. Bailey DB Jr., Raspa M, Olmsted M, Holiday DB, Co-occurring conditions associated with FMR1 gene variations: Findings from a national parent survey. Am. J. Med. Genet. A 146A, 2060–2069 (2008). [PubMed: 18570292]
2. Budimirovic DB, Kaufmann WE, What can we learn about autism from studying fragile X syndrome? Dev. Neurosci 33, 379–394 (2011). [PubMed: 21893949]
3. Hagerman RJ, Berry-Kravis E, Kaufmann WE, Ono MY, Tartaglia N, Lachiewicz A, Kronk R, Delahunty C, Hessl D, Visootsak J, Picker J, Gane L, Tranfaglia M, Advances in the treatment of fragile X syndrome. Pediatrics 123, 378–390 (2009). [PubMed: 19117905]
4. Song FJ, Barton P, Sleightholme V, Yao GL, Fry-Smith A, Screening for fragile X syndrome: A literature review and modelling study. Health Technol. Assess 7, 1–106 (2003).
5. Turner G, Webb T, Wake S, Robinson H, Prevalence of fragile X syndrome. Am. J. Med. Genet64, 196–197 (1996). [PubMed: 8826475]
6. Bhakar AL, Dölen G, Bear MF, The pathophysiology of fragile X (and what it teaches us about synapses). Annu. Rev. Neurosci 35, 417–443 (2012). [PubMed: 22483044]
7. Till SM, Asiminas A, Jackson AD, Katsanevaki D, Barnes SA, Osterweil EK, Bear MF, Chattarji S, Wood ER, Wyllie DJ, Kind PC, Conserved hippocampal cellular pathophysiology but distinct behavioural deficits in a new rat model of FXS. Hum. Mol. Genet 24, 5977–5984 (2015). [PubMed: 26243794]
8. Richter JD, Bassell GJ, Klann E, Dysregulation and restoration of translational homeostasis in fragile X syndrome. Nat. Rev. Neurosci 16, 595–605 (2015). [PubMed: 26350240]
9. Krueger DD, Bear MF, Toward fulfilling the promise of molecular medicine in fragile X syndrome. Annu. Rev. Med 62, 411–429 (2011). [PubMed: 21090964]
10. Bear MF, Huber KM, Warren ST, The mGluR theory of fragile X mental retardation. Trends Neurosci. 27, 370–377 (2004). [PubMed: 15219735]
11. Scharf SH, Jaeschke G, Wettstein JG, Lindemann L, Metabotropic glutamate receptor 5 as drug target for fragile X syndrome. Curr. Opin. Pharmacol 20, 124–134 (2015). [PubMed: 25488569]
12. Berry-Kravis E, Des Portes V, Hagerman R, Jacquemont S, Charles P, Visootsak J, Brinkman M, Rerat K, Koumaras B, Zhu L, Barth GM, Jaecklin T, Apostol G, von Raison F, Mavoglurant in

fragile X syndrome: Results of two randomized, double-blind, placebo-controlled trials. Sci. Transl. Med 8, 321ra325 (2016).

13. Yan QJ, Rammal M, Tranfaglia M, Bauchwitz RP, Suppression of two major fragile X syndrome mouse model phenotypes by the mGluR5 antagonist MPEP. Neuropharmacology 49, 1053–1066 (2005). [PubMed: 16054174]
14. Homayoun H, Stefani MR, Adams BW, Tamagan GD, Moghaddam B, Functional interaction between NMDA and mGlu5 receptors: Effects on working memory, instrumental learning, motor behaviors, and dopamine release. Neuropsychopharmacology 29, 1259–1269 (2004). [PubMed: 15010696]
15. Pietraszek M, Gravius A, Schäfer D, Weil T, Trifanova D, Danysz W, mGluR5, but not mGluR1, antagonist modifies MK-801-induced locomotor activity and deficit of prepulse inhibition. Neuropharmacology 49, 73–85 (2005). [PubMed: 15992582]
16. Pecknold JC, McClure DJ, Appeltauer L, Wrzesinski L, Allan T, Treatment of anxiety using fenobam (a nonbenzodiazepine) in a double-blind standard (diazepam) placebo-controlled study. J. Clin. Psychopharmacol 2, 129–133 (1982). [PubMed: 7042771]
17. Porter RH, Jaeschke G, Spooren W, Ballard TM, Buttelmann B, Kolczewski S, Peters JU, Prinssen E, Wichmann J, Vieira E, Muhlemann A, Gatti S, Mutel V, Malherbe P, Fenobam: A clinically validated nonbenzodiazepine anxiolytic is a potent, selective, and noncompetitive mGlu5 receptor antagonist with inverse agonist activity. J. Pharmacol. Exp. Ther 315, 711–721 (2005). [PubMed: 16040814]
18. Abou Farha K, Bruggeman R, Baljé-Volkers C, Metabotropic glutamate receptor 5 negative modulation in phase I clinical trial: Potential impact of circadian rhythm on the neuropsychiatric adverse reactions-do hallucinations matter? ISRN Psychiatry 2014, 652750(2014). [PubMed: 24729909]
19. Min WW, Yuskaitis CJ, Yan Q, Sikorski C, Chen S, Jope RS, Bauchwitz RP, Elevated glycogen synthase kinase-3 activity in fragile X mice: Key metabolic regulator with evidence for treatment potential. Neuropharmacology 56, 463–472 (2009). [PubMed: 18952114]
20. Yuskaitis CJ, Mines MA, King MK, Sweatt JD, Miller CA, Jope RS, Lithium ameliorates altered glycogen synthase kinase-3 and behavior in a mouse model of fragile X syndrome. Biochem. Pharmacol 79, 632–646 (2010). [PubMed: 19799873]
21. Mines MA, Jope RS, Glycogen synthase kinase-3: A promising therapeutic target for fragile X syndrome. Front. Mol. Neurosci 4, 35 (2011). [PubMed: 22053151]
22. Choi CH, Schoenfeld BP, Bell AJ, Hinchey P, Kollaros M, Gertner MJ, Woo NH, Tranfaglia MR, Bear MF, Zukin RS, McDonald TV, Jongens TA, McBride SM, Pharmacological reversal of synaptic plasticity deficits in the mouse model of fragile X syndrome by group II mGluR antagonist or lithium treatment. Brain Res. 1380, 106–119 (2011). [PubMed: 21078304]
23. Liu ZH, Huang T, Smith CB, Lithium reverses increased rates of cerebral protein synthesis in a mouse model of fragile X syndrome. Neurobiol. Dis 45, 1145–1152 (2012). [PubMed: 22227453]
24. McBride SM, Choi CH, Wang Y, Liebelt D, Braunstein E, Ferreiro D, Sehgal A, Siwicki KK, Dockendorff TC, Nguyen HT, McDonald TV, Jongens TA, Pharmacological rescue of synaptic plasticity, courtship behavior, and mushroom body defects in a *Drosophila* model of fragile X syndrome. Neuron 45, 753–764 (2005). [PubMed: 15748850]
25. Chang S, Bray SM, Li Z, Zarnescu DC, He C, Jin P, Warren ST, Identification of small molecules rescuing fragile X syndrome phenotypes in Drosophila. Nat. Chem. Biol 4, 256–263 (2008). [PubMed: 18327252]
26. Jope RS, Lithium and GSK-3: One inhibitor, two inhibitory actions, multiple outcomes. Trends Pharmacol. Sci 24, 441–443 (2003). [PubMed: 12967765]
27. Portis S, Giunta B, Obregon D, Tan J, The role of glycogen synthase kinase-3 signaling in neurodevelopment and fragile X syndrome. Int. J. Physiol. Pathophysiol. Pharmacol 4, 140–148 (2012). [PubMed: 23071871]
28. Berry-Kravis E, Sumis A, Hervey C, Nelson M, Porges SW, Weng N, Weiler IJ, Greenough WT, Open-label treatment trial of lithium to target the underlying defect in fragile X syndrome. J. Dev. Behav. Pediatr 29, 293–302 (2008). [PubMed: 18698192]

29. Siegel M, Beresford CA, Bunker M, Verdi M, Vishnevetsky D, Karlsson C, Teer O, Stedman A, Smith KA, Preliminary investigation of lithium for mood disorder symptoms in children and adolescents with autism spectrum disorder. J. Child Adolesc. Psychopharmacol 24, 399–402 (2014). [PubMed: 25093602]
30. Bhat R, Xue Y, Berg S, Hellberg S, Ormo M, Nilsson Y, Radesäter AC, Jerning E, Markgren PO, Borgegård T, Nylof M, Giménez-Cassina A, Hernández F, Lucas JJ, Díaz-Nido J, Avila J, Structural insights and biological effects of glycogen synthase kinase 3-specific inhibitor AR-A014418. J. Biol. Chem 278, 45937–45945 (2003). [PubMed: 12928438]
31. Coghlan MP, Culbert AA, Cross DA, Corcoran SL, Yates JW, Pearce NJ, Rausch OL, Murphy GJ, Carter PS, Roxbee Cox L, Mills D, Brown MJ, Haigh D, Ward RW, Smith DG, Murray KJ, Reith AD, Holder JC, Selective small molecule inhibitors of glycogen synthase kinase-3 modulate glycogen metabolism and gene transcription. Chem. Biol 7, 793–803 (2000). [PubMed: 11033082]
32. O'Leary O, Nolan Y, Glycogen synthase kinase-3 as a therapeutic target for cognitive dysfunction in neuropsychiatric disorders. CNS Drugs 29, 1–15 (2015). [PubMed: 25380674]
33. Wagner FF, Bishop JA, Gale JP, Shi X, Walk M, Ketterman J, Patnaik D, Barker D, Walpita D, Campbell AJ, Nguyen S, Lewis M, Ross L, Weïwer M, An WF, Germain AR, Nag PP, Metkar S, Kaya T, Dandapani S, Olson DE, Barbe AL, Lazzaro F, Sacher JR, Cheah JH, Fei D, Perez J, Munoz B, Palmer M, Stegmaier K, Schreiber SL, Scolnick E, Zhang YL, Haggarty SJ, Holson EB, Pan JQ, Inhibitors of glycogen synthase kinase 3 with exquisite kinome-wide selectivity and their functional effects. ACS Chem. Biol 11, 1952–1963 (2016). [PubMed: 27128528]
34. Morin PJ, β-Catenin signaling and cancer. Bioessays 21, 1021–1030 (1999). [PubMed: 10580987]
35. Hall AP, Escott KJ, Sanganee H, Hickling KC, Preclinical toxicity of AZD7969: Effects of GSK3beta inhibition in adult stem cells. Toxicol. Pathol 43, 384–399 (2015). [PubMed: 25326587]
36. Jiang Y, Dai J, Zhang H, Sottnik JL, Keller JM, Escott KJ, Sanganee HJ, Yao Z, McCauley LK, Keller ET, Activation of the Wnt pathway through AR79, a GSK3β inhibitor, promotes prostate cancer growth in soft tissue and bone. Mol. Cancer Res 11, 1597–1610 (2013). [PubMed: 24088787]
37. Huang RY, Hsieh KP, Huang WW, Yang YH, Use of lithium and cancer risk in patients with bipolar disorder: Population-based cohort study. Br. J. Psychiatry 209, 393–399 (2016). [PubMed: 27388574]
38. Martinsson L, Westman J, Hallgren J, Osby U, Backlund L, Lithium treatment and cancer incidence in bipolar disorder. Bipolar Disord. 18, 33–40 (2016). [PubMed: 26880208]
39. Beurel E, Grieco SF, Jope RS, Glycogen synthase kinase-3 (GSK3): Regulation, actions, and diseases. Pharmacol. Ther 148, 114–131 (2015). [PubMed: 25435019]
40. Woodgett JR, Molecular cloning and expression of glycogen synthase kinase-3/factor A. EMBO J. 9, 2431–2438 (1990). [PubMed: 2164470]
41. Dajani R, Fraser E, Roe SM, Young N, Good V, Dale TC, Pearl LH, Crystal structure of glycogen synthase kinase 3 beta: Structural basis for phosphate-primed substrate specificity and autoinhibition. Cell 105, 721–732 (2001). [PubMed: 11440715]
42. Kaidanovich-Beilin O, Woodgett JR, GSK-3: Functional insights from cell biology and animal models. Front. Mol. Neurosci 4, 40 (2011). [PubMed: 22110425]
43. Kaidanovich-Beilin O, Lipina TV, Takao K, van Eede M, Hattori S, Laliberte C, Khan M, Okamoto K, Chambers JW, Fletcher PJ, MacAulay K, Doble BW, Henkelman M, Miyakawa T, Roder J, Woodgett JR, Abnormalities in brain structure and behavior in GSK-3alpha mutant mice. Mol. Brain 2, 35 (2009). [PubMed: 19925672]
44. Hoeflich KP, Luo J, Rubie EA, Tsao MS, Jin O, Woodgett JR, Requirement for glycogen synthase kinase-3beta in cell survival and NF-κB activation. Nature 406, 86–90 (2000). [PubMed: 10894547]
45. MacAulay K, Doble BW, Patel S, Hansotia T, Sinclair EM, Drucker DJ, Nagy A, Woodgett JR, Glycogen synthase kinase 3α-specific regulation of murine hepatic glycogen metabolism. Cell Metab. 6, 329–337 (2007). [PubMed: 17908561]
46. Doble BW, Patel S, Wood GA, Kockeritz LK, Woodgett JR, Functional redundancy of GSK-3alpha and GSK-3beta in Wnt/beta-catenin signaling shown by using an allelic series of embryonic stem cell lines. Dev. Cell 12, 957–971 (2007). [PubMed: 17543867]

47. Wagner FF, Benajiba L, Campbell AJ, Weiwer M, Sacher JR, Gale JP, Ross L, Puissant A, Alexe G, Conway A, Back M, Pikman Y, Galinsky I, DeAngelo DJ, Stone RM, Kaya T, Shi X, Robers MB, Machleidt T, Wilkinson J, Hermine O, Kung A, Stein AJ, Lakshminarasimhan D, Hemann MT, Scolnick E, Zhang YL, Pan JQ, Stegmaier K, Holson EB, Exploiting an Asp-Glu "switch" in glycogen synthase kinase 3 to design paralog-selective inhibitors for use in acute myeloid leukemia. Sci. Transl. Med 10, eaam8460 (2018). [PubMed: 29515000]

48. Michalon A, Sidorov M, Ballard TM, Ozmen L, Spooren W, Wettstein JG, Jaeschke G, Bear MF, Lindemann L, Chronic pharmacological mGlu5 inhibition corrects fragile X in adult mice. Neuron 74, 49–56 (2012). [PubMed: 22500629]

49. Osterweil EK, Chuang SC, Chubykin AA, Sidorov M, Bianchi R, Wong RK, Bear MF, Lovastatin corrects excess protein synthesis and prevents epileptogenesis in a mouse model of fragile X syndrome. Neuron 77, 243–250 (2013). [PubMed: 23352161]

50. Dolen G, Osterweil E, Rao BS, Smith GB, Auerbach BD, Chattarji S, Bear MF, Correction of fragile X syndrome in mice. Neuron 56, 955–962 (2007). [PubMed: 18093519]

51. Osterweil EK, Krueger DD, Reinhold K, Bear MF, Hypersensitivity to mGluR5 and ERK1/2 leads to excessive protein synthesis in the hippocampus of a mouse model of fragile X syndrome. J. Neurosci 30, 15616–15627 (2010). [PubMed: 21084617]

52. Qin M, Kang J, Burlin TV, Jiang C, Smith CB, Postadolescent changes in regional cerebral protein synthesis: An in vivo study in the FMR1 null mouse. J. Neurosci 25, 5087–5095 (2005). [PubMed: 15901791]

53. Guo W, Molinaro G, Collins KA, Hays SA, Paylor R, Worley PF, Szumlinski KK, Huber KM, Selective disruption of metabotropic glutamate receptor 5-homer interactions mimics phenotypes of fragile X syndrome in mice. J. Neurosci 36, 2131–2147 (2016). [PubMed: 26888925]

54. Hays SA, Huber KM, Gibson JR, Altered neocortical rhythmic activity states in Fmr1 KO mice are due to enhanced mGluR5 signaling and involve changes in excitatory circuitry. J. Neurosci 31, 14223–14234 (2011). [PubMed: 21976507]

55. Haider B, McCormick DA, Rapid neocortical dynamics: Cellular and network mechanisms. Neuron 62, 171–189 (2009). [PubMed: 19409263]

56. Sanchez-Vives MV, McCormick DA, Cellular and network mechanisms of rhythmic recurrent activity in neocortex. Nat. Neurosci 3, 1027–1034 (2000). [PubMed: 11017176]

57. Peineau S, Nicolas CS, Bortolotto ZA, Bhat RV, Ryves WJ, Harwood AJ, Dournaud P, Fitzjohn SM, Collingridge GL, A systematic investigation of the protein kinases involved in NMDA receptor-dependent LTD: Evidence for a role of GSK-3 but not other serine/threonine kinases. Mol. Brain 2, 22 (2009). [PubMed: 19583853]

58. Bradley CA, Peineau S, Taghibiglou C, Nicolas CS, Whitcomb DJ, Bortolotto ZA, Kaang BK, Cho K, Wang YT, Collingridge GL, A pivotal role of GSK-3 in synaptic plasticity. Front. Mol. Neurosci 5, 13 (2012). [PubMed: 22363262]

59. Phiel CJ, Wilson CA, Lee VM, Klein PS, GSK-3α regulates production of Alzheimer's disease amyloid-β peptides. Nature 423, 435–439 (2003). [PubMed: 12761548]

60. Rockenstein E, Torrance M, Adame A, Mante M, Bar-on P, Rose JB, Crews L, Masliah E, Neuroprotective effects of regulators of the glycogen synthase kinase-3β signaling pathway in a transgenic model of Alzheimer's disease are associated with reduced amyloid precursor protein phosphorylation. J. Neurosci 27, 1981–1991 (2007). [PubMed: 17314294]

61. Qin M, Kang J, Smith CB, Increased rates of cerebral glucose metabolism in a mouse model of fragile X mental retardation. Proc. Natl. Acad. Sci. U.S.A 99, 15758–15763 (2002). [PubMed: 12427968]

62. Awad H, Hubert GW, Smith Y, Levey AI, Conn PJ, Activation of metabotropic glutamate receptor 5 has direct excitatory effects and potentiates NMDA receptor currents in neurons of the subthalamic nucleus. J. Neurosci 20, 7871–7879 (2000). [PubMed: 11050106]

63. Chen HH, Liao PF, Chan MH, mGluR5 positive modulators both potentiate activation and restore inhibition in NMDA receptors by PKC dependent pathway. J. Biomed. Sci 18, 19 (2011). [PubMed: 21342491]

64. Doherty AJ, Palmer MJ, Henley JM, Collingridge GL, Jane DE, (RS)-2-chloro-5-hydroxyphenylglycine (CHPG) activates mGlu5, but no mGlu1, receptors expressed in CHO cells

and potentiates NMDA responses in the hippocampus. Neuropharmacology 36, 265–267 (1997). [PubMed: 9144665]

65. Mannaioni G, Marino MJ, Valenti O, Traynelis SF, Conn PJ, Metabotropic glutamate receptors 1 and 5 differentially regulate CA1 pyramidal cell function. J. Neurosci 21, 5925–5934 (2001). [PubMed: 11487615]
66. Naisbitt S, Kim E, Tu JC, Xiao B, Sala C, Valtschanoff J, Weinberg RJ, Worley PF, Sheng M, Shank, a novel family of postsynaptic density proteins that binds to the NMDA receptor/PSD-95/GKAP complex and cortactin. Neuron 23, 569–582 (1999). [PubMed: 10433268]
67. Pisani A, Gubellini P, Bonsi P, Conquet F, Picconi B, Centonze D, Bernardi G, Calabresi P, Metabotropic glutamate receptor 5 mediates the potentiation of *N*-methyl-D-aspartate responses in medium spiny striatal neurons. Neuroscience 106, 579–587 (2001). [PubMed: 11591458]
68. Rook JM, Xiang Z, Lv X, Ghoshal A, Dickerson JW, Bridges TM, Johnson KA, Foster DJ, Gregory KJ, Vinson PN, Thompson AD, Byun N, Collier RL, Bubser M, Nedelcovych MT, Gould RW, Stauffer SR, Daniels JS, Niswender CM, Lavreysen H, Mackie C, Conde-Ceide S, Alcazar J, Bartolome-Nebreda JM, Macdonald GJ, Talpos JC, Steckler T, Jones CK, Lindsley CW, Conn PJ, Biased mGlu5-positive allosteric modulators provide in vivo efficacy without potentiating mGlu5 modulation of NMDAR currents. Neuron 86, 1029–1040 (2015). [PubMed: 25937172]
69. Tu JC, Xiao B, Naisbitt S, Yuan JP, Petralia RS, Brakeman P, Doan A, Aakalu VK, Lanahan AA, Sheng M, Worley PF, Coupling of mGluR/Homer and PSD-95 complexes by the Shank family of postsynaptic density proteins. Neuron 23, 583–592 (1999). [PubMed: 10433269]
70. Ugolini A, Corsi M, Bordi F, Potentiation of NMDA and AMPA responses by group I mGluR in spinal cord motoneurons. Neuropharmacology 36, 1047–1055 (1997). [PubMed: 9294969]
71. Cosford ND, Tehrani L, Roppe J, Schweiger E, Smith ND, Anderson J, Bristow L, Brodkin J, Jiang X, McDonald I, Rao S, Washburn M, Varney MA, 3-[(2-Methyl-1,3-thiazol-4-yl)ethynyl]-pyridine: A potent and highly selective metabotropic glutamate subtype 5 receptor antagonist with anxiolytic activity. J. Med. Chem 46, 204–206 (2003). [PubMed: 12519057]
72. Dolen G, Bear MF, Role for metabotropic glutamate receptor 5 (mGluR5) in the pathogenesis of fragile X syndrome. J. Physiol 586, 1503–1508 (2008). [PubMed: 18202092]
73. Chuang SC, Zhao W, Bauchwitz R, Yan Q, Bianchi R, Wong RK, Prolonged epileptiform discharges induced by altered group I metabotropic glutamate receptor-mediated synaptic responses in hippocampal slices of a fragile X mouse model. J. Neurosci 25, 8048–8055 (2005). [PubMed: 16135762]
74. Banko JL, Hou L, Poulin F, Sonenberg N, Klann E, Regulation of eukaryotic initiation factor 4E by converging signaling pathways during metabotropic glutamate receptor-dependent long-term depression. J. Neurosci 26, 2167–2173 (2006). [PubMed: 16495443]
75. Pop AS, Levenga J, de Esch CE, Buijsen RA, Nieuwenhuizen IM, Li T, Isaacs A, Gasparini F, Oostra BA, Willemsen R, Rescue of dendritic spine phenotype in Fmr1 KO mice with the mGluR5 antagonist AFQ056/Mavoglurant. Psychopharmacology (Berl) 231, 1227–1235 (2014). [PubMed: 23254376]
76. de Esch CE, van den Berg WE, Buijsen RA, Jaafar IA, Nieuwenhuizen-Bakker IM, Gasparini F, Kushner SA, Willemsen R, Fragile X mice have robust mGluR5-dependent alterations of social behaviour in the Automated Tube Test. Neurobiol. Dis 75, 31–39 (2015). [PubMed: 25562659]
77. Gantois I, Khoutorsky A, Popic J, Aguilar-Valles A, Freemantle E, Cao R, Sharma V, Pooters T, Nagpal A, Skalecka A, Truong VT, Wiebe S, Groves IA, Jafarnejad SM, Chapat C, McCullagh EA, Gamache K, Nader K, Lacaille JC, Gkogkas CG, Sonenberg N, Metformin ameliorates core deficits in a mouse model of fragile X syndrome. Nat. Med 23, 674–677 (2017). [PubMed: 28504725]
78. Gallagher SM, Daly CA, Bear MF, Huber KM, Extracellular signal-regulated protein kinase activation is required for metabotropic glutamate receptor-dependent long-term depression in hippocampal area CA1. J. Neurosci 24, 4859–4864 (2004). [PubMed: 15152046]
79. Huber KM, Kayser MS, Bear MF, Role for rapid dendritic protein synthesis in hippocampal mGluR-dependent long-term depression. Science 288, 1254–1256 (2000). [PubMed: 10818003]

80. Huber KM, Roder JC, Bear MF, Chemical induction of mGluR5- and protein synthesis–dependent long-term depression in hippocampal area CA1. J. Neurophysiol 86, 321–325 (2001). [PubMed: 11431513]
81. Chen X, Sun W, Pan Y, Yang Q, Cao K, Zhang J, Zhang Y, Chen M, Chen F, Huang Y, Dai L, Chen S, Lithium ameliorates open-field and elevated plus maze behaviors, and brain phospho-glycogen synthase kinase 3-β expression in fragile X syndrome model mice. Neurosciences 18, 356–362 (2013). [PubMed: 24141459]
82. King MK, Jope RS, Lithium treatment alleviates impaired cognition in a mouse model of fragile X syndrome. Genes Brain Behav. 12, 723–731 (2013). [PubMed: 23941202]
83. Liu ZH, Chuang DM, Smith CB, Lithium ameliorates phenotypic deficits in a mouse model of fragile X syndrome. Int. J. Neuropsychopharmacol 14, 618–630 (2011). [PubMed: 20497624]
84. Pardo M, Beurel E, Jope RS, Cotinine administration improves impaired cognition in the mouse model of fragile X syndrome. Eur. J. Neurosci 45, 490–498 (2017). [PubMed: 27775852]
85. Guo W, Murthy AC, Zhang L, Johnson EB, Schaller EG, Allan AM, Zhao X, Inhibition of GSK3β improves hippocampus-dependent learning and rescues neurogenesis in a mouse model of fragile X syndrome. Hum. Mol. Genet 21, 681–691 (2012). [PubMed: 22048960]
86. Pardo M, Cheng Y, Velmeshev D, Magistri M, Eldar-Finkelman H, Martinez A, Faghihi MA, Jope RS, Beurel E, Intranasal siRNA administration reveals IGF2 deficiency contributes to impaired cognition in fragile X syndrome mice. JCI Insight 2, e91782 (2017). [PubMed: 28352664]
87. Sutherland C, What are the bona fide GSK3 substrates? Int. J. Alzheimers Dis 2011, 505607 (2011). [PubMed: 21629754]
88. Westmark CJ, Chuang SC, Hays SA, Filon MJ, Ray BC, Westmark PR, Gibson JR, Huber KM, Wong RK, APP causes hyperexcitability in fragile X mice. Front. Mol. Neurosci 9, 147 (2016). [PubMed: 28018172]
89. Fang X, Yu SX, Lu Y, Bast RC Jr., J. R. Woodgett, G. B. Mills, Phosphorylation and inactivation of glycogen synthase kinase 3 by protein kinase A. Proc. Natl. Acad. Sci. U.S.A 97, 11960–11965 (2000). [PubMed: 11035810]
90. Ronesi JA, Collins KA, Hays SA, Tsai NP, Guo W, Birnbaum SG, Hu JH, Worley PF, Gibson JR, Huber KM, Disrupted Homer scaffolds mediate abnormal mGluR5 function in a mouse model of fragile X syndrome. Nat. Neurosci 15, 431–440 (2012). [PubMed: 22267161]
91. Choi CH, Schoenfeld BP, Bell AJ, Hinchey J, Rosenfelt C, Gertner MJ, Campbell SR, Emerson D, Hinchey P, Kollaros M, Ferrick NJ, Chambers DB, Langer S, Sust S, Malik A, Terlizzi AM, Liebelt DA, Ferreiro D, Sharma A, Koenigsberg E, Choi RJ, Louneva N, Arnold SE, Featherstone RE, Siegel SJ, Zukin RS, McDonald TV, Bolduc FV, Jongens TA, McBride SM, Multiple drug treatments that increase cAMP signaling restore long-term memory and aberrant signaling in fragile X syndrome models. Front. Behav. Neurosci 10, 136 (2016). [PubMed: 27445731]
92. Udagawa T, Farny NG, Jakovcevski M, Kaphzan H, Alarcon JM, Anilkumar S, Ivshina M, Hurt JA, Nagaoka K, Nalavadi VC, Lorenz LJ, Bassell GJ, Akbarian S, Chattarji S, Klann E, Richter JD, Genetic and acute CPEB1 depletion ameliorate fragile X pathophysiology. Nat. Med 19, 1473–1477 (2013). [PubMed: 24141422]
93. Qin M, Huang T, Kader M, Krych L, Xia Z, Burlin T, Zeidler Z, Zhao T, Smith CB, R-Baclofen reverses a social behavior deficit and elevated protein synthesis in a mouse model of fragile X syndrome. Int. J. Neuropsychopharmacol 18, pyv034 (2015). [PubMed: 25820841]
94. Jacquemont S, Pacini L, Jonch AE, Cencelli G, Rozenberg I, He Y, D'Andrea L, Pedini G, Eldeeb M, Willemsen R, Gasparini F, Tassone F, Hagerman R, Gomez-Mancilla B, Bagni C, Protein synthesis levels are increased in a subset of individuals with fragile X syndrome. Hum. Mol. Genet 27, 3825 (2018). [PubMed: 30107584]
95. Darnell JC, Van Driesche SJ, Zhang C, Hung KY, Mele A, Fraser CE, Stone EF, Chen C, Fak JJ, Chi SW, Licatalosi DD, Richter JD, Darnell RB, FMRP stalls ribosomal translocation on mRNAs linked to synaptic function and autism. Cell 146, 247–261 (2011). [PubMed: 21784246]
96. Stoppel LJ, Osterweil EK, Bear MF, in Fragile X Syndrome, Wilemsen R, Kooy RF, Eds. (Academic Press, 2017), chap. 9, pp. 173–204.
97. Asiminas A, Jackson AD, Louros SR, Till SM, Spano T, Dando O, Bear MF, Chattarji S, Hardingham GE, Osterweil EK, Wyllie DJA, Wood ER, Kind PC, Sustained correction of

associative learning deficits after brief, early treatment in a rat model of fragile X Syndrome. Sci. Transl. Med 11, eaao0498 (2019). [PubMed: 31142675]

98. Thomson SR, Seo SS, Barnes SA, Louros SR, Muscas M, Dando O, Kirby C, Wyllie DJA, Hardingham GE, Kind PC, Osterweil EK, Cell-type-specific translation profiling reveals a novel strategy for treating fragile X syndrome. Neuron 95, 550–563.e5 (2017). [PubMed: 28772121]
99. Cooke SK, Russin J, Moulton K, Nadel J, Loutaev I, Gu Q, Li Z, Smith CB, Effects of the presence and absence of amino acids on translation, signaling, and long-term depression in hippocampal slices from Fmr1 knockout mice. J. Neurochem 151, 764–776 (2019). [PubMed: 31539452]
100. Mullard A, Fragile X disappointments upset autism ambitions. Nat. Rev. Drug Discov 14, 151–153 (2015). [PubMed: 25722228]
101. Schaefer TL, Davenport MH, Grainger LM, Robinson CK, Earnheart AT, Stegman MS, Lang AL, Ashworth AA, Molinaro G, Huber KM, Erickson CA, Acamprosate in a mouse model of fragile X syndrome: Modulation of spontaneous cortical activity, ERK1/2 activation, locomotor behavior, and anxiety. J. Neurodev. Disord 9, 6 (2017). [PubMed: 28616095]
102. Agmon A, Connors BW, Thalamocortical responses of mouse somatosensory (barrel) cortex in vitro. Neuroscience 41, 365–379 (1991). [PubMed: 1870696]
103. Gibson JR, Bartley AF, Hays SA, Huber KM, Imbalance of neocortical excitation and inhibition and altered UP states reflect network hyperexcitability in the mouse model of fragile X syndrome. J. Neurophysiol 100, 2615–2626 (2008). [PubMed: 18784272]
104. Dudek SM, Bear MF, Homosynaptic long-term depression in area CA1 of hippocampus and effects of *N*-methyl-D-aspartate receptor blockade. Proc. Natl. Acad. Sci. U.S.A 89, 4363–4367 (1992). [PubMed: 1350090]
105. O'Callaghan JP, Sriram K, Focused microwave irradiation of the brain preserves in vivo protein phosphorylation: Comparison with other methods of sacrifice and analysis of multiple phosphoproteins. J. Neurosci. Methods 135, 159–168 (2004). [PubMed: 15020100]
106. Wang Y, Zhang Y, Hu W, Xie S, Gong C-X, Iqbal K, Liu F, Rapid alteration of protein phosphorylation during postmortem: Implication in the study of protein phosphorylation. Sci. Rep 5, 15709 (2015). [PubMed: 26511732]
107. Pan JQ, Lewis MC, Ketterman JK, Clore EL, Riley M, Richards KR, Berry-Scott E, Liu X, Wagner FF, Holson EB, Neve RL, Biechele TL, Moon RT, Scolnick EM, Petryshen TL, Haggarty SJ, AKT kinase activity is required for lithium to modulate mood-related behaviors in mice. Neuropsychopharmacology 36, 1397–1411 (2011). [PubMed: 21389981]

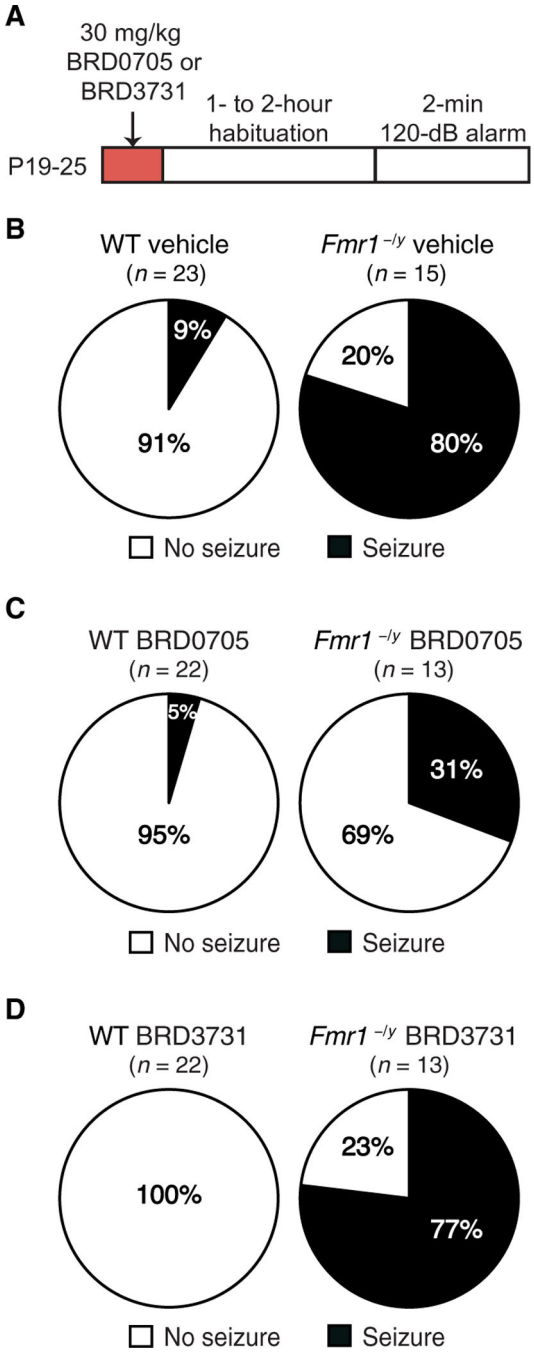

Fig. 1. Acute administration of BRD0705 but not BRD3731 reduces audiogenic seizure incidence in *Fmr1*$^{-/y}$ mice.

(**A**) Schematic shows dose schedule and audiogenic seizure (AGS) timeline (P, postnatal day). (**B**) Vehicle-treated *Fmr1*$^{-/y}$ mice ($n = 15$) exhibited enhanced susceptibility to AGS in response to an auditory alarm cosmpared with wild-type (WT) control mice ($n = 23$; $P = 0.001$, two-tailed Fisher's exact test). (**C**) Acute intraperitoneal administration of BRD0705 (30 mg/kg; GSK3α inhibitor) had no effect on seizure incidence in WT mice ($n = 22$; $P = 1.0$, two-tailed Fisher's exact test) but significantly reduced the incidence of AGS in *Fmr1*$^{-/y}$

mice compared with vehicle ($n = 13$; $P = 0.02$, two-tailed Fisher's exact test). (**D**) Acute intraperitoneal administration of BRD3731 (30 mg/kg; GSK3β inhibitor) did not affect seizure incidence in either WT ($n = 22$) or *Fmr1*$^{-/y}$ mice ($n = 13$; $P = 1.0$, two-tailed Fisher's exact test).

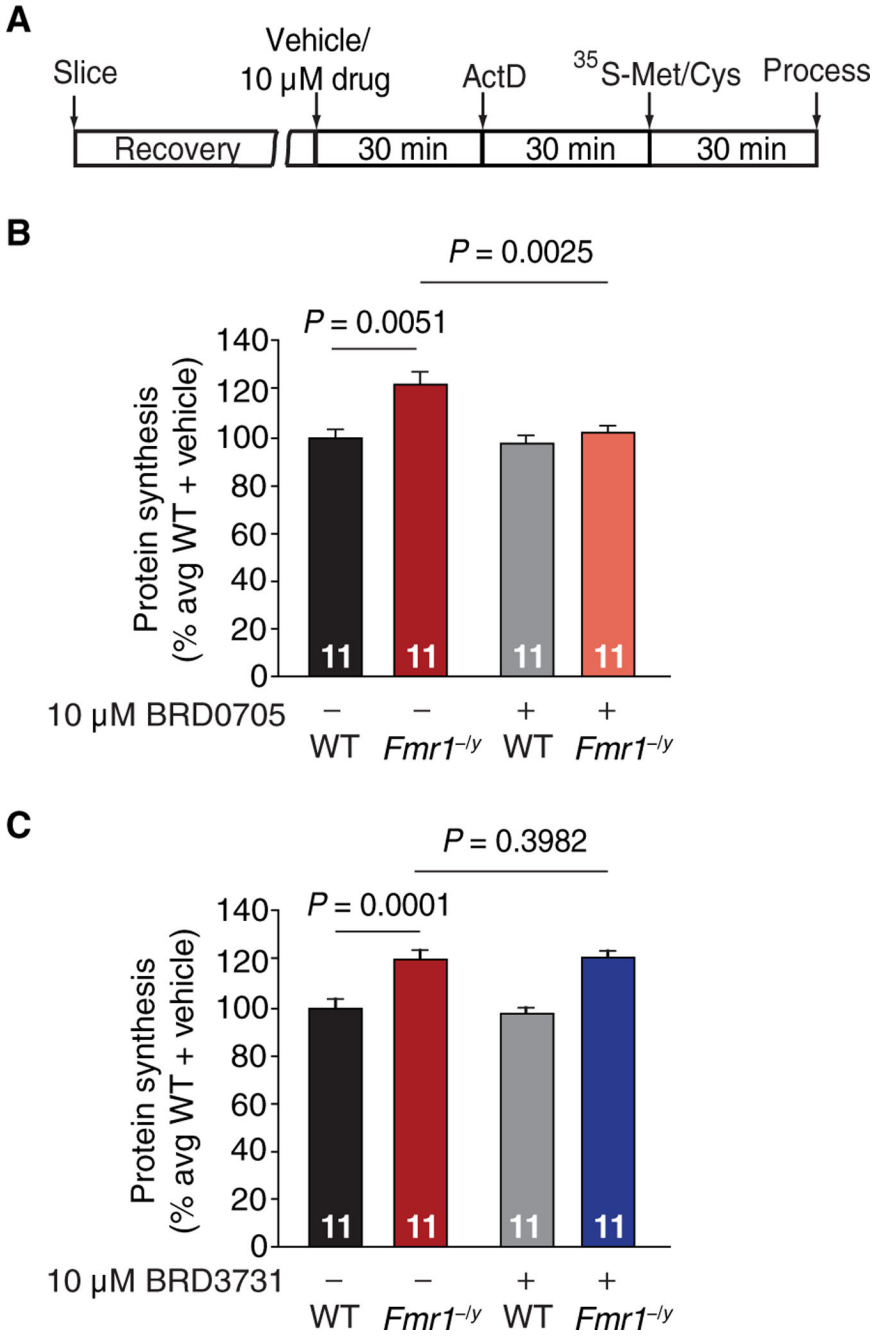

Fig. 2. BRD0705 but not BRD3731 corrects elevated protein synthesis in *Fmr1*$^{-/y}$ mice.

(**A**) Timeline of experiments to measure basal incorporation of radio-labeled Met/Cys into protein in mouse hippocampal slices. (**B**) Basal protein synthesis was increased in hippocampal slices from *Fmr1*$^{-/y}$ mice compared to wild-type (WT) mice. Treatment with BRD0705 (10 μM) reduced elevated protein synthesis in *Fmr1*$^{-/y}$ mice back to WT levels. There was no interaction between treatment and genotype in a two-way ANOVA [$F(1,40) = 3.783$, $P = 0.0588$]; however, there was a main effect of genotype and of treatment [$F(1,40) = 8.78$, $P = 0.0051$; $F(1,40) = 10.46$, $P = 0.0025$]. (**C**) Basal protein synthesis was increased in hippocampal slices from *Fmr1*$^{-/y}$ mice compared to WT mice and treatment with

BRD3731 (10 μM) had no effect. There was no interaction between treatment and genotype in a two-way ANOVA [F1,40) = 0.059, P = 0.8087]; however, there was a main effect of genotype, but not of treatment [F(1,40) = 40.02, P = 0.0001; F(1,40) = 0.7249, P = 0.3982]. Numbers within each bar indicate the number of animals in each group; data are displayed as mean ± SEM.

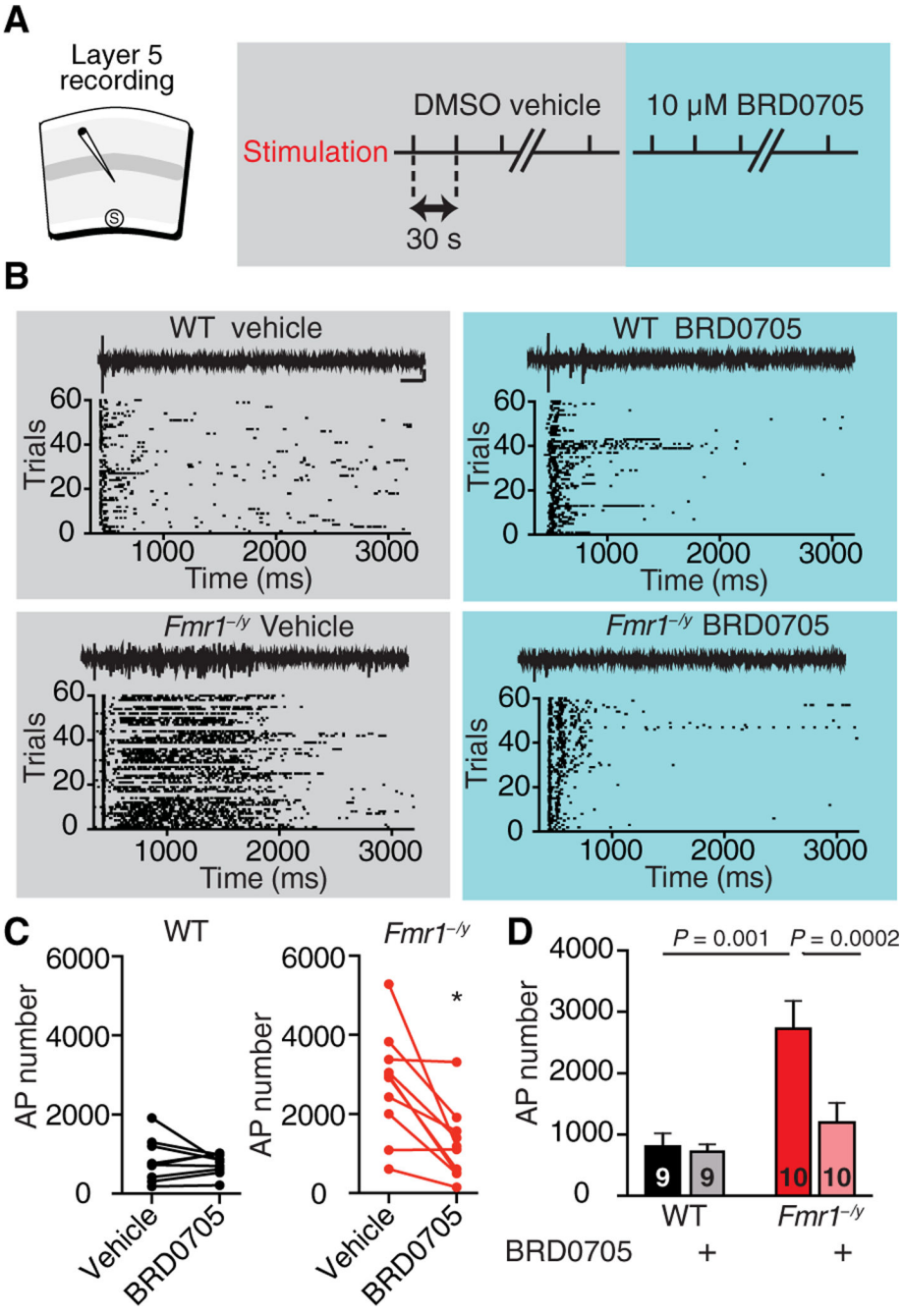

Fig. 3. BRD0705 reduces evoked hyperexcitability in the *Fmr1*$^{-/y}$ visual cortex.

(**A**) Extracellular recordings were performed in layer 5 of the visual cortex. Action potentials were generated with white matter stimulation every 30 s for a total of 60 trials with vehicle, followed by 60 trials with 10 μM BRD0705. (**B**) Representative raster plots and traces from both wild-type (WT) and *Fmr1*$^{-/y}$ mouse visual cortical slices show prolonged firing in the *Fmr1*$^{-/y}$ slices, which was corrected by BRD0705 treatment. Scale bar, 200 μV by 200 ms. (**C**) BRD0705 (10 μM) treatment significantly reduced the number of action potentials (APs) in *Fmr1*$^{-/y}$ visual cortical slices (*$P = 0.007$, paired t test), but had no effect on WT visual cortical slices ($P = 0.5848$, paired t test). (**D**) Mean number of APs was significantly greater

in *Fmr1*$^{-/y}$ slices and could be corrected by application of 10 μM BRD0705 [two-way repeated measures ANOVA, genotype × treatment, $F(1,17) = 10.54$, $P = 0.0047$, WT vehicle versus *Fmr1*$^{-/y}$ vehicle, $P = 0.0001$, *Fmr1*$^{-/y}$ vehicle versus *Fmr1*$^{-/y}$ + BRD0705, $P = 0.002$]. Numbers within each bar indicate the number of animals in each group; data in (D) are displayed as mean ± SEM.

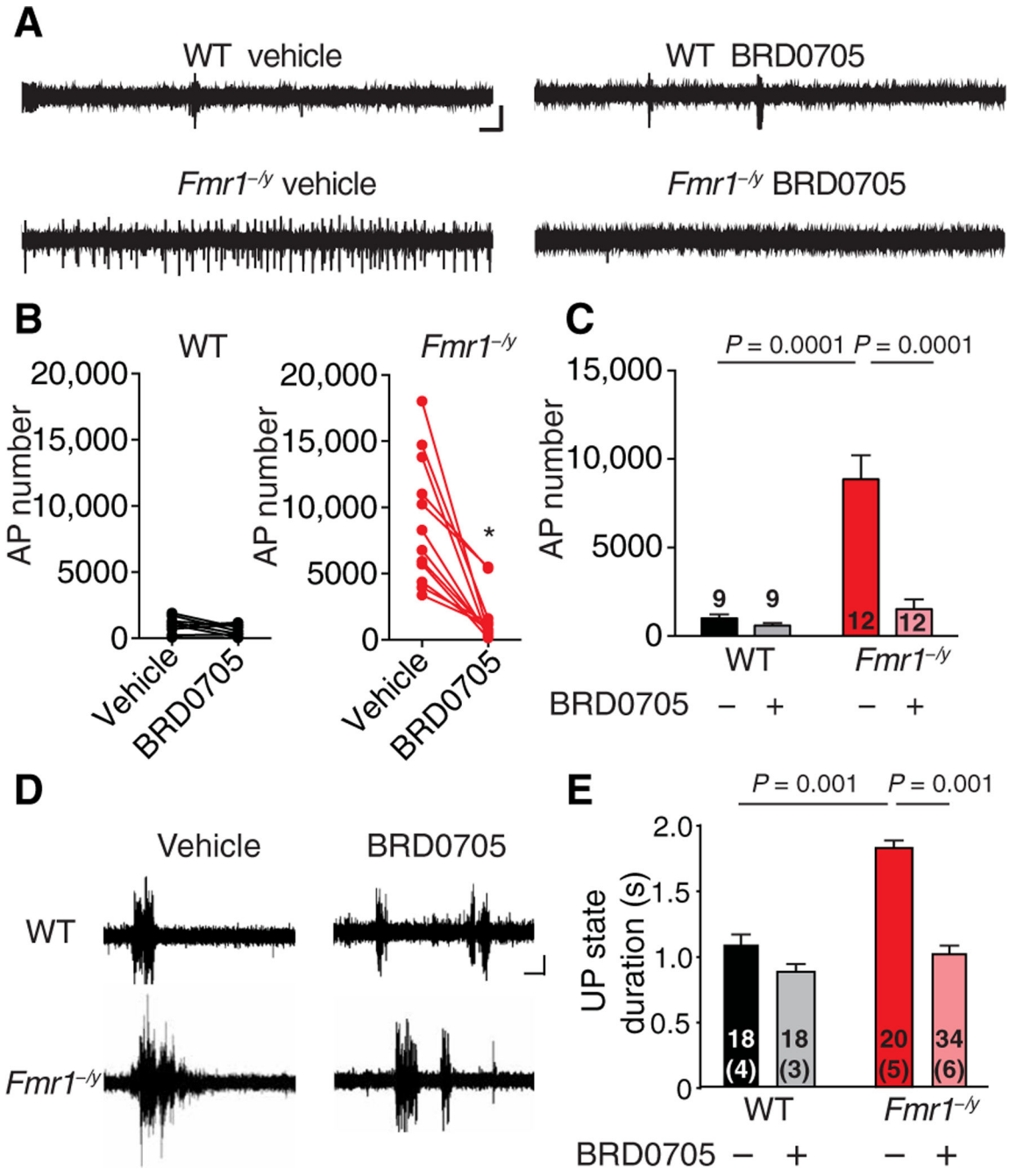

Fig. 4. BRD0705 reduces elevated spontaneous activity in the *Fmr1*$^{-/y}$ sensory neocortex.

(**A**) Sample traces from vehicle-treated and BRD0705-treated slices of visual cortex from wild-type (WT) and *Fmr1*$^{-/y}$ mice are shown. Scale bar, 200 μV by 1 s. (**B**) BRD0705 (10 μM) treatment significantly reduced the number of spontaneous action potentials (APs) in *Fmr1*$^{-/y}$ slices (**P* = 0.0003, paired *t* test). (**C**) Mean number of spontaneous action potentials was greater in *Fmr1*$^{-/y}$ slices and could be corrected by application of 10 μM BRD0705 [two-way repeated measures ANOVA, genotype × treatment, $F(1,19) = 18.09$, $P = 0.0004$, WT vehicle versus *Fmr1*$^{-/y}$ vehicle, $P = 0.0001$, *Fmr1*$^{-/y}$ vehicle versus *Fmr1*$^{-/y}$ + BRD0705, **P* = 0.0001, WT vehicle versus *Fmr1*$^{-/y}$ + BRD0705, $P = 0.459$]. Number of

animals is indicated by numbers within each bar. (**D**) Shown are sample traces of extracellular multiunit recordings from layer 4 of acute cortical slices prepared from WT or *Fmr1*$^{-/y}$ somatosensory cortex and preincubated in either DMSO vehicle or BRD0705 (25 μM). Scale bar, 0.15 mV by 1 s. (**E**) The mean UP state duration was greater in *Fmr1*$^{-/y}$ slices and could be corrected by application of BRD0705 [two-way ANOVA, genotype × treatment, $F(1,86) = 13.63$, $P = 0.0004$, and post hoc Sidak's multiple comparisons, WT DMSO versus *Fmr1*$^{-/y}$ DMSO, $P = 0.001$, *Fmr1*$^{-/y}$ DMSO versus *Fmr1*$^{-/y}$ BRD0705, $P = 0.001$]. Statistical comparisons of UP state duration were performed using the number of slices as *n*, indicated in each bar, as described previously (54). Number of animals is indicated parenthetically; data in (C) and (E) are displayed as mean ± SEM.

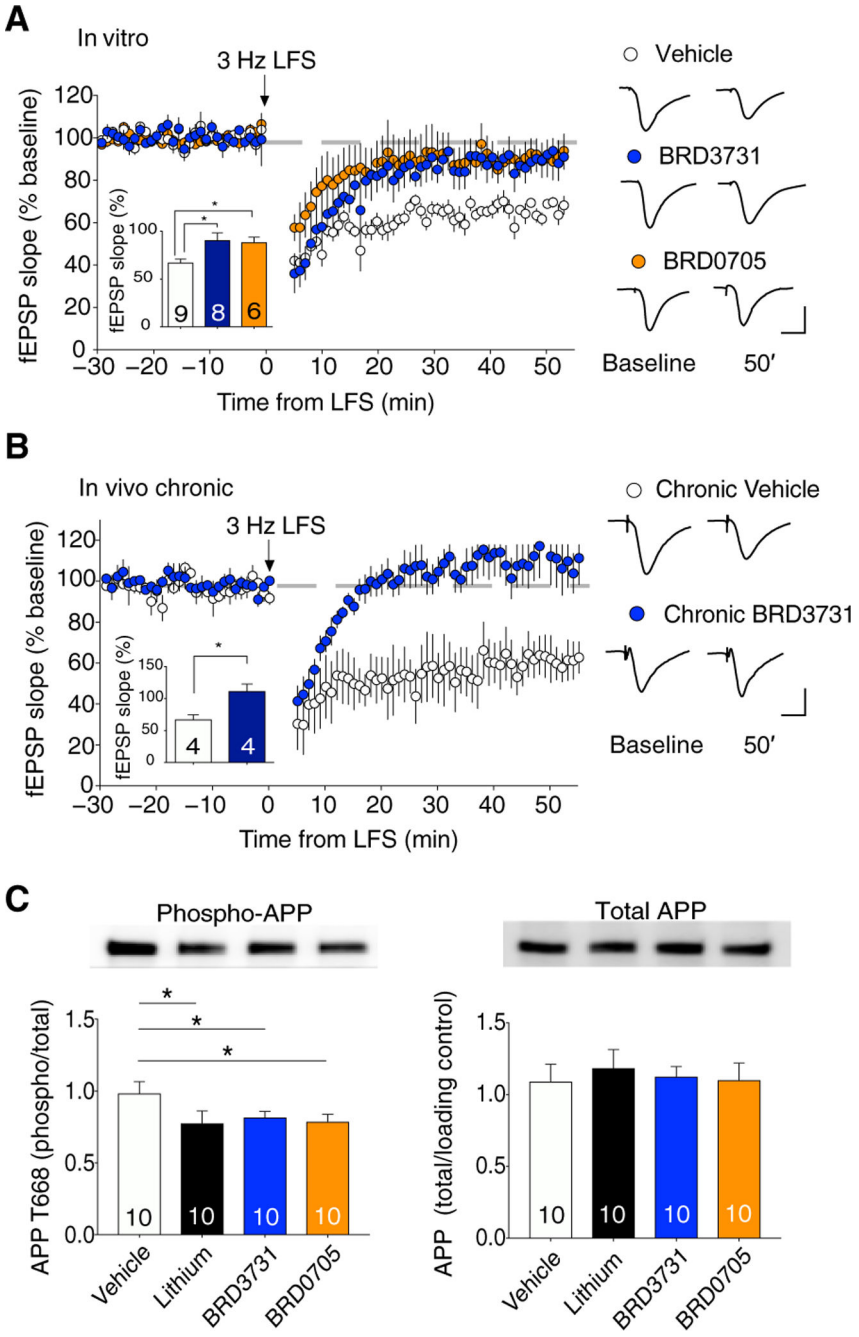

Fig. 5. Acute and chronic GSK3 inhibition blocks hippocampal NMDAR- dependent LTD.

(**A**) Field excitatory postsynaptic potentials (fEPSPs) were recorded from hippocampal slices from the CA1 dendritic layer of wild-type (WT) mice in response to Schaffer collateral stimulation. LTD was induced with 900 pulses at 3-Hz low-frequency stimulation (LFS) in hippocampal slices incubated in 0.09% DMSO vehicle, BRD3731 (10 μM), or BRD0705 (10 μM). Inset shows summary data of the magnitude of LTD (normalized to baseline) measured at 50 min after low-frequency stimulation. Acute application of both BRD3731 and BRD0705 blocked low-frequency stimulation–induced LTD in WT mice (numbers of animals are indicated within each bar). There was a significant effect of

treatment in a one-way ANOVA [$F(2,20) = 5.807$; $P = 0.023$]. Shown are the average field potential waveforms during the artificial cerebrospinal fluid treatment baseline, and 50 min after low-frequency stimulation. Scale bar, 5 ms/500 μV. (**B**) Compared to vehicle-treated animals, chronic dosing in vivo with the GSK3β inhibitor BRD3731 inhibited NMDAR-dependent LTD in hippocampal slices ex vivo. BRD3731 (30 mg/kg) was injected intraperitoneally daily for five consecutive days, and transverse slices of hippocampus were prepared 1 hour after the last injection. Summary data of LTD (normalized to baseline) for both chronic BRD3731-treated ($n = 4$) and vehicle-treated ($n = 4$) animals are shown in the inset (BRD3731 versus vehicle $P = 0.0175$, Student's two-tailed t test). Average field potential waveforms during baseline and post-LTD induction with 900 pulses at 3 Hz (LFS) are shown. Scale bar, 5 ms/500 μV. (**C**) *Fmr1*$^{-/y}$ animals received intraperitoneal daily injections for five consecutive days of either vehicle, BRD3731 [30 mg/kg ip, once daily (QD)], BRD0705 (30 mg/kg ip, QD), or lithium chloride (60 mg/kg ip, twice daily); the right dorsal hippocampus was dissected 1 hour after the final dose for analysis of GSK3-dependent phosphorylation. Western blot analysis of lysates from dorsal hippocampus showed reduced APP phosphorylation in response to treatment with either BRD0705, BRD3731, or lithium chloride [one-way ANOVA, $F(3,37) = 3.918$, $P = 0.0159$]. Chronic GSK3 inhibition had no effect on total APP protein [one-way ANOVA, $F(3,40) = 0.1419$, $P = 0.9343$]. Data are displayed as mean ± SEM.

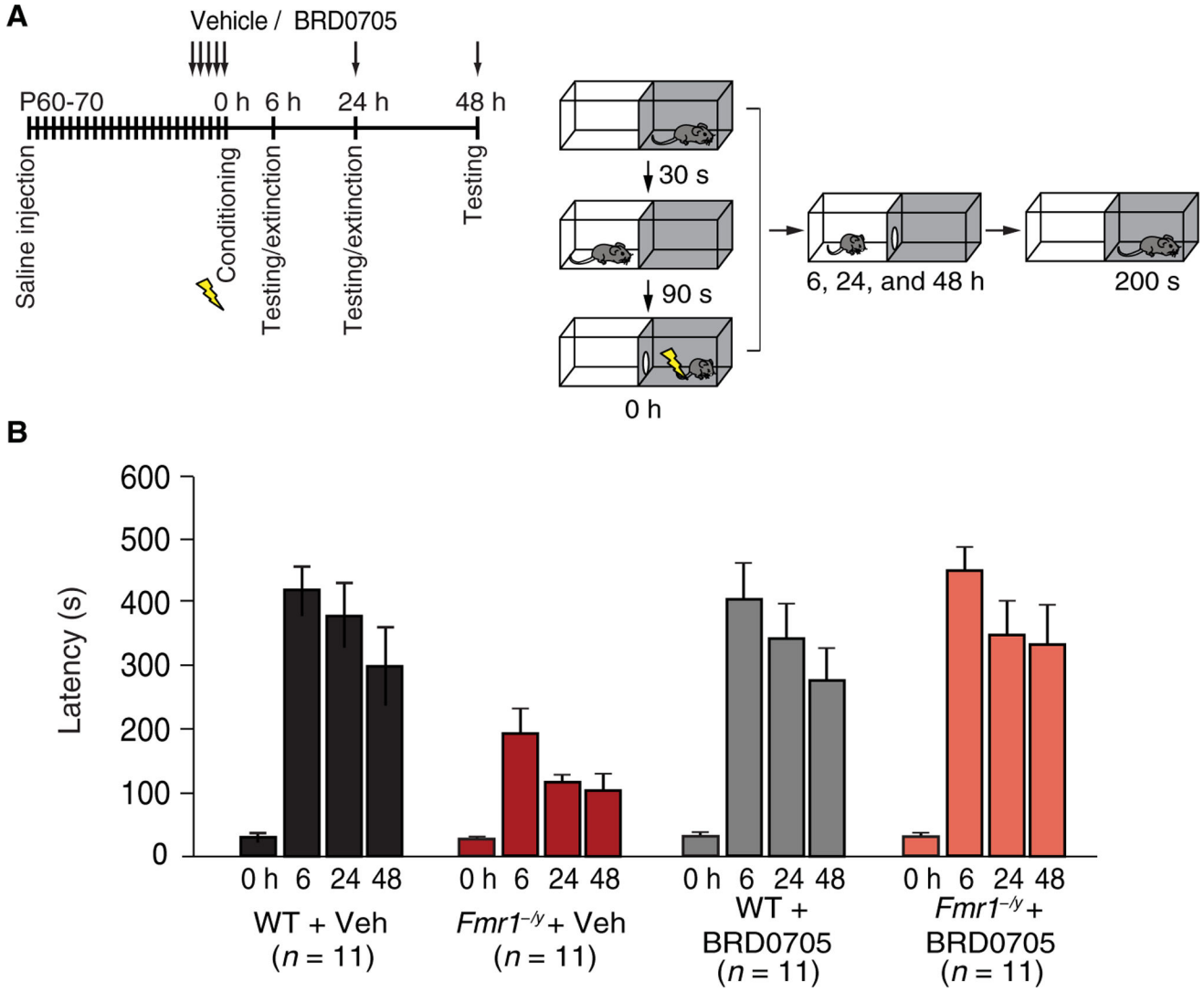

Fig. 6. Inhibition of GSK3α in *Fmr1*$^{-/y}$ mice corrects impaired memory in an inhibitory avoidance learning task.

(**A**) Experimental design of dosing schedule and inhibitory avoidance learning task. Animals were dosed with saline for 20 days before vehicle or drug to habituate them to the injection. After 5 days of vehicle or drug, animals began the inhibitory avoidance task, receiving a daily dose of vehicle or drug throughout the remainder of the experiment. (**B**) Quantification of the latency of mice to freely enter the dark side of the box assayed at several time points after fear conditioning. There was a statistically significant interaction between genotype and time point across treatments [repeated measures three-way ANOVA with Greenhouse-Geisser correction, $F(3,120) = 4.180$, $P = 0.0075$]. Vehicle-treated *Fmr1*$^{-/y}$ mice showed impaired acquisition of inhibitory avoidance learning compared to vehicle-treated wild-type mice (WT vehicle versus *Fmr1*$^{-/y}$ vehicle, Tukey's posttest; at time 0 hour, $P = 0.99$; at 6 hours, $P = 0.035$; at 24 hours, $P = 0.01$; at 48 hours, $P = 0.280$). BRD0705-treated *Fmr1*$^{-/y}$ mice (30 mg/kg ip) showed comparable acquisition and extinction of inhibitory avoidance compared to vehicle-treated and BRD0705-treated WT mice (WT BRD0705 versus *Fmr1*$^{-/y}$ BRD0705, Tukey's posttest; $P > 0.99$ at all time points) and showed improvement compared

to vehicle-treated *Fmr1*$^{-/y}$ mice (*Fmr1*$^{-/y}$ vehicle versus *Fmr1*$^{-/y}$ BRD0705, Tukey's posttest; at time 0 hour, $P = 0.99$; at 6 hours, $P = 0.01$; at 24 hours, $P = 0.06$; at 48 hours, $P = 0.17$; $n = 11$ animals in each of the four groups). Data are displayed as mean ± SEM.

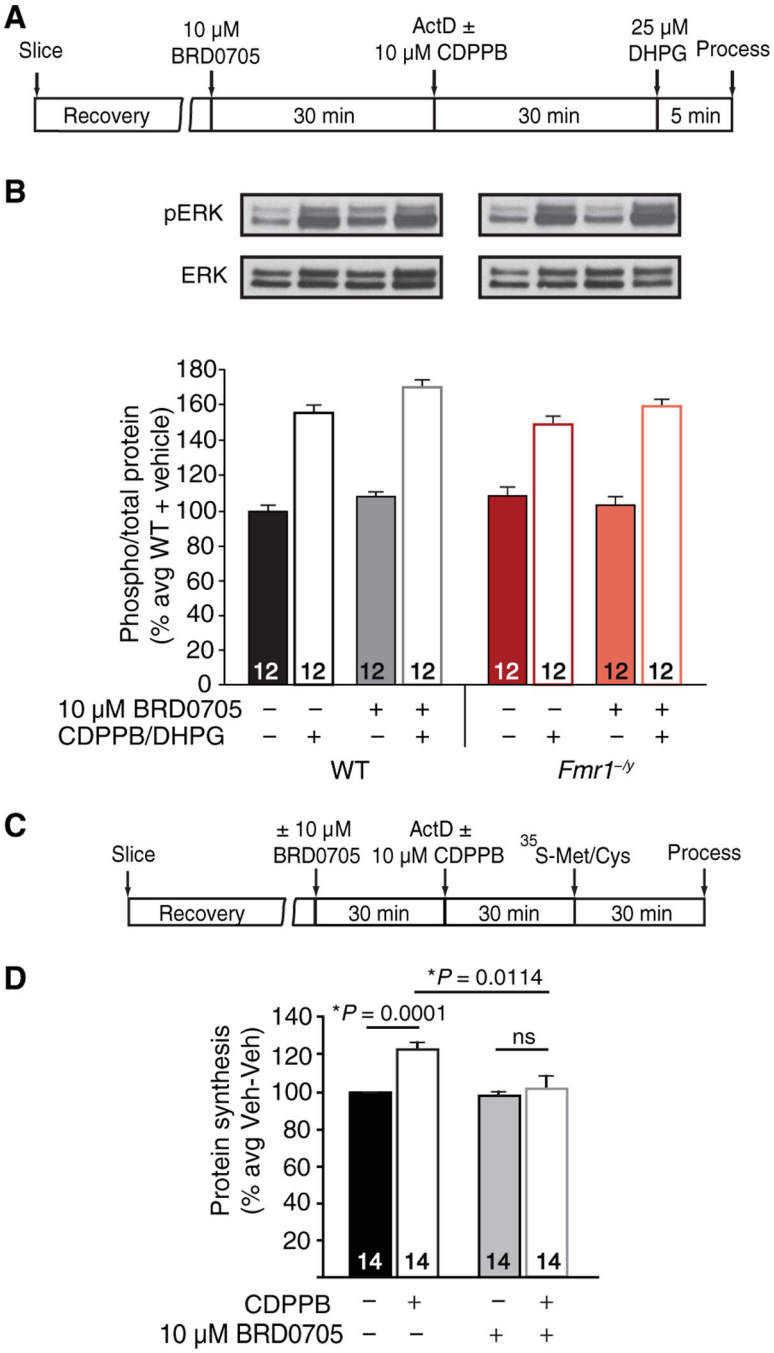

Fig. 7. Inhibition of GSK3α reduces mGluR5-stimulated protein synthesis but not ERK1/2 pathway activation.

(**A**) Schematic illustrates experimental timeline for ERK1/2 assay. (**B**) Activation of mGluR5 caused a robust phosphorylation of ERK1/2 across all conditions. There was no significant interaction between genotype, drug and stimulation in a three-way ANOVA [$F(1,88) = 0.657$, $P = 0.420$]; however, there was a main effect of stimulation [$F(1,88) = 362.035$, $P = 0.0001$] but no main effect for genotype [$F(1,88) = 0.965$, $P = 0.329$] and no significant interaction between genotype and stimulation [$F(1,88) = 3.191$, $P = 0.077$] or drug and stimulation [$F(1,88) = 2.509$, $P = 0.117$]. Although there was a small but

significant main effect of drug treatment [$F(1,88) = 4.727$, $P = 0.032$], there was no decrease in ERK phosphorylation with BRD0705 treatment, and there was no significant interaction between genotype and drug treatment [$F(1,88) = 3.279$, $P = 0.074$]. Numbers of animals are indicated within each bar. (**C**) Schematic illustrates experimental timeline for protein synthesis assay (also see Materials and Methods). (**D**) Stimulation of mGluR5 with 3-cyano-*N*-(1,3-diphenyl-1*H*-pyrazol-5-yl)benzamide (CDPPB; 10 μM) significantly increased protein synthesis in hippocampal slices from wild-type (WT) mice compared with vehicle (Veh), and this effect was blocked by BRD0705. There was a significant interaction between stimulation and BRD0705 treatment in a two-way repeated measures ANOVA [$F(3,52) = 6.656$, $P = 0.023$; paired *t* test: WT vehicle versus WT CDPPB, $P = 0.0001$]. Treatment with BRD0705 (10 μM) blocked the elevation in protein synthesis (WT vehicle versus WT CDPPB + BRD0705: $^{*}P = 0.578$; WT CDPPB versus WT CDPPB + BRD0705: $^{*}P = 0.0114$, paired *t* test). Data are displayed as mean ± SEM. ns, not significant.

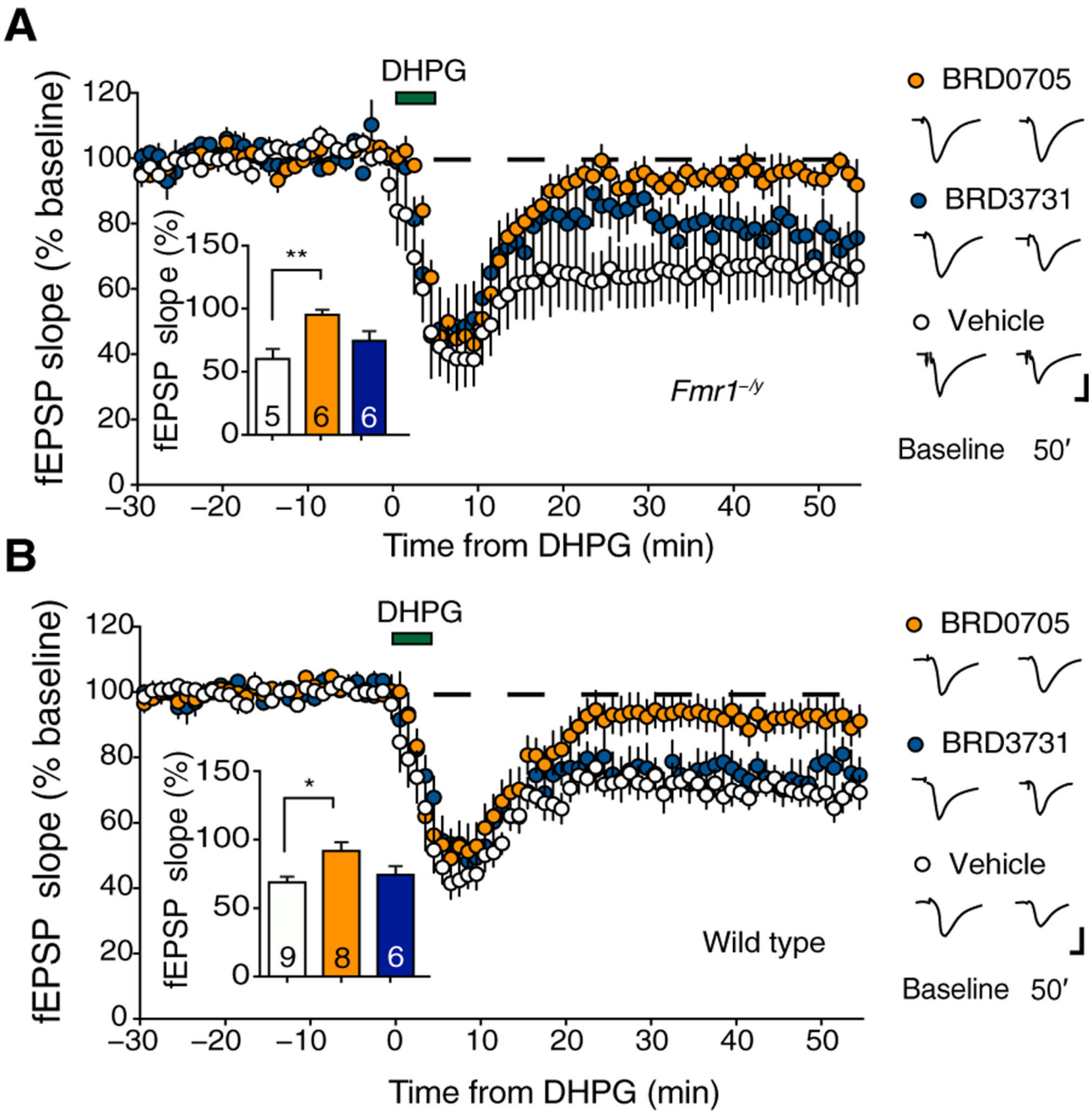

Fig. 8. mGluR-dependent LTD in the hippocampus is sensitive to inhibition of GSK3α but not GSK3β.

Field excitatory postsynaptic potentials (fEPSPs) were recorded in the CA1 hippocampal dendritic layer in response to Schaffer collateral stimulation. Protein synthesis–dependent and mGluR-dependent LTD were induced by applying 3,5-dihydroxyphenylglycine (DHPG; 100 μM, 5 min) to acutely prepared hippocampal slices from *Fmr1*$^{-/y}$ and wild-type (WT) mouse littermates. GSK3 inhibitors were applied to the slices for the duration of recording. BRD0705, but not BRD3731, blocked induction of LTD in hippocampal slices from *Fmr1*$^{-/y}$ mice (A) and their WT littermates (B). (**A**) Summary data of the average fEPSP slope from *Fmr1*$^{-/y}$ mouse hippocampal slices (normalized to baseline) measured at 50 min after DHPG

treatment is shown in the inset (number of animals is indicated within each bar). There was a significant effect of treatment in a one-way ANOVA [$F(2,14) = 8.617$, $P = 0.0036$; Bonferroni's posttest vehicle versus BRD0705, $P = 0.003$; vehicle versus BRD3731, $P = 0.342$]. The average field potential waveforms during baseline and post DHPG treatment are shown. Scale bar, 5 ms/500 μV. (**B**) Summary data of the average fEPSP slope from WT mouse hippocampal slices (normalized to baseline) measured at 50 min after DHPG treatment is shown in the inset (number of animals is indicated within each bar). There was a significant effect of treatment in a one-way ANOVA [$F(2,20) = 6.69$, $P = 0.0006$; Bonferroni's posttest vehicle versus BRD0705, $P = 0.006$; vehicle versus BRD3731, $P = 0.999$]. The average field potential waveforms during baseline and after DHPG treatment are shown. Scale bar, 5 ms/500 μV. Data are displayed as mean ± SEM.